INFRARED LASER SPECTROSCOPY OF WATER CONTAINING CLUSTERS IN HELIUM NANODROPLETS

by

STEVEN DOUGLAS FLYNN

(Under the Direction of GARY ELLIOTT DOUBERLY)

ABSTRACT

Helium nanodroplets were used as a host to isolate mixed $(HCl)_m(H_2O)_n$ and Ne-$(H_2O)_n$ clusters. These clusters were probed with infrared (IR) laser spectroscopy. For $(HCl)_m(H_2O)_n$ clusters the H-Cl stretch region is probed and vibrational bands are definitively assigned to the structures responsible for them through the use of pick-up cell (PUC) dependence studies, optically selective mass spectrometry (OSMS), vibrational transition moment angle (VTMA) measurements, and comparisons with theoretical predictions. In a similar manner, a new higher energy small water cluster has been observed and characterized spectroscopically. This new observation of a theoretically predicted structure of water was achieved by adding a Ne atom to the nanodroplet prior to the pick-up of water.

INDEX WORDS: "Small water clusters; HENDI; $(H_2O)_m(HCl)_n$; Acid dissociation; $(H_2O)_n$-Ne"

INFRARED LASER SPECTROSCOPY OF WATER CONTAINING CLUSTERS IN HELIUM NANODROPLETS

by

STEVEN DOUGLAS FLYNN

B.S. Chemistry, North Carolina State University, 2007

A Thesis Submitted to the Graduate Faculty of The University of Georgia in Partial Fulfillment of the Requirements for the Degree

MASTERS OF SCIENCE

ATHENS, GEORGIA

2013

INFRARED LASER SPECTROSCOPY OF WATER CONTAINING CLUSTERS IN HELIUM NANODROPLETS

by

STEVEN DOUGLAS FLYNN

Major Professor: Gary Elliott Douberly

Committee: Geoffrey Smith

Michael Duncan

Electronic Version Approved:

Maureen Grasso
Dean of the Graduate School
The University of Georgia
May 2013

DEDICATION

Mom and Dad

Thank you so much.

ACKNOWLEDGEMENTS

Thank God

TABLE OF CONTENTS

Page

LIST OF TABLES

Page

LIST OF FIGURES

Page

CHAPTER 1

INTRODCUTION

He Nanodroplets and their Use for Spectroscopy

Helium, below its lambda point, exists as a superfluid with bulk properties that still are not well understood, especially on the nanoscale, despite the fact that the properties of bulk helium have been of interest since it was first liquefied in 1908.[1] Superfluid He can be formed as droplets through free jet expansion, as shown first by Becker *et. al*. in 1961.[2] Bulk helium exists as a superfluid when it is below its lambda point at 2.17K.[1] These droplets can get even colder through evaporation ultimately reaching temperatures of approximately 0.37 K for ^{4}He.[3]

Droplets of superfluid ^{4}He atoms, with sizes ranging from several hundred to 10^9 atoms, depending on nozzle conditions, travel from the source towards the detector at a speed of ~350 m/s.[4] The properties of the droplets are not completely known, but through the early investigation of these droplets it was eventually realized that they could serve as an "ultimate matrix" to contain an atom, molecule, or cluster for spectroscopic investigation.[5] The work presented in this thesis involves making heterogeneous molecular clusters in the helium nanodroplets, and the spectroscopic characterization of these clusters.

History

First, it is necessary to acknowledge the work of George Pimentel *et al* for their discovery of cryogenic matrix isolation in 1954.[6] As mentioned above Becker was

responsible for the first free-jet expansion of He in 1961.[2] The discovery of the pick-up technique which is used in all of the presented experiments came from Scoles and his group in 1985.[7] The first spectroscopy of a solute molecule within a He droplet was demonstrated by Goyal *et a.l* in 1992, as they probed the SF_6 molecule with infrared (IR) spectroscopy and a line tunable CO_2 laser.[8] The ν_3 band was compared to experimental results of SF_6 in an Ar matrix.[9,10,11] Because of the increased resolution over solid matrix studies the potential of He nanodroplets to be of great importance to the spectroscopic community was demonstrated. Later Fröchtenicht *et al.* used a continuous wave diode laser to provide the first rotationally resolved spectrum of SF_6 in a He nanodroplet. The spectrum revealed that the SF_6 molecular symmetry was preserved, thus answering the prevailing question of whether a molecule resides on the surface of a droplet or within. The preserved symmetry indicated that the molecule resides near the center of the droplet. This study also showed that one can use a gas phase Hamiltonian to describe the spectrum, as long as the B rotational constant is lowered to about a third of the gas phase constant.[4] Prior to these experimental measurements, theoretical studies suggested a droplet temperature of about 0.4 K.[12] The relative IR band intensities from the SF ν_3 spectrum provided an experimental value of 0.37 K.[13] Toennies and co-workers pioneered scattering and inelastic collision studies that lead to much of our current understanding of the physical properties of He nanodroplets.[5] The name for the new technique is helium nanodroplet isolation spectroscopy (HENDI).

Stienkemeier and Lehmann wrote of Roger Miller in a 2006 review article that "much of the present knowledge about helium nanodroplets results from the work of Roger Miller…" Miller, and his group, published a large number of spectroscopic

studies of radicals and biomolecules in He nanodroplets.[14] Many He droplet techniques were pioneered in the Miller group including pendular state spectroscopy, the vibrational transition moment angle technique (VTMA), and optically selective mass spectrometry (OSMS).[4] Among many other contributions, Vilesov, and co-workers, have done much of the pulsed droplet beam work.[5]

Are He Nanodroplets the "Ideal Matrix"?

Helium nanodroplets provide a near perfect matrix for the investigation of doped species.[5] Because of the low temperature, the resolution of spectra in helium nanodroplets compared to other, solid, matrices is much higher.[4] Another advantage is that species of low vapor pressure can be studied in He droplets because the detection is so sensitive. In the He droplet experiments a form of action spectroscopy is used, which depends on the cross sectional area of the average droplet. The pressures required to dope the droplets are very low compared to the density of molecules required to attenuate light. Since most gas phase experiments detect the attenuation of light, the pressures of the target molecule are usually quite high. Therefore, an advantage HENDI has over typical gas phase experiments is that lower vapor pressures of the spectroscopic target can be used.[14] The spectra of molecules isolated in solid matrices tend to exhibit inhomogeneous broadening due to strong dopant-matrix interactions.[5] In HENDI the interactions between the droplet and the dopant are not so strong resulting in much smaller shifts from gas phase values. Another advantage of He droplet spectroscopy over solid matrix spectroscopy is that a He solvated molecule can rotate, while a guest molecule in a solid matrix does not. When using quantum mechanics to predict or

analyze a spectrum, as shown later in this thesis, the gas phase Hamiltonian can be used and the only constant that really needs to be altered is the B value.[4]

One review article states that helium nanodroplets are the "ultimate" matrix since they are characterized by "extremely low temperatures, small matrix broadening, and they offer the opportunity to form new molecular complexes."[5] In addition He droplet spectroscopy has is that the droplets are transparent to light from the far infrared all the way to the vacuum UV range of the electromagnetic spectrum.[5] This advantage for spectroscopy is also one of the biggest problems in determining He nanodroplet properties, and is the biggest reason so little is known about He nanodroplets themselves. In addition, almost any chromophore can be loaded into a droplet beam via a scattering cell placed along the He beam path, this has created a totally new class of spectroscopic experiments.[15]

Also of advantage is that the cluster has a finite size where as a solid matrix has a much larger area where it is difficult to control cluster aggregation. There are also no problems with surface aggregation, which means different surface structures compared to the internal matrix structures, when using HENDI. Having vastly different surface structures, relative to the bulk frozen sample, is a common problem with the interpretation of spectra of molecules embedded in solid matrices.[15]

The HENDI method is, however, an experimentally difficult method by which to obtain spectra. The alignment of everything must be perfect, the pumping speeds must be sufficient, and the start-up cost is high. Also as a negative point, the spectra of molecules in He droplets are not as sharp as those from gas phase molecules. The true properties of the droplets are difficult to know precisely, so there are corrections that are used that can

be a little vague such as the droplet sizes, the droplet temperature, and the consistency of doping the droplets.

A disadvantage of He droplets compared to solid matrices is that the beam is in motion and the solid matrix is stationary. The ability to hold samples static in a solid matrix for days is advantageous for methods such as Fourier transform infrared spectroscopy (FTIR), which is currently not possible in He nanodroplets.[15] Also, a solid matrix has fine temperature control that doesn't exist with He droplets. He droplets remain at about 0.37 K without the ability to anneal or change temperatures.

HCl-H_2O

The dissociation mechanism of HCl in aqueous media is a fundamental problem in chemical physics and remains an active area of research.[16] A fundamental question motivating these studies is how many water molecules it takes to pry apart HCl to form a solvent separated ion pair $H^+(H_2O)_nCl^-$. This seemingly simple question has proved to be a challenge for both theory and experiment. One approach to this problem is to study the structure of small clusters composed of HCl and water and look for the signatures of dissociation. An infrared spectroscopic study of mixed $(HCl)_m(H_2O)_n$ clusters grown in the low temperature environment of a helium nanodroplet is reported herein.[17] A somewhat non-traditional version of Stark spectroscopy is employed to arrive at unambiguous assignments of cluster bands in the HCl stretch region of the spectrum.

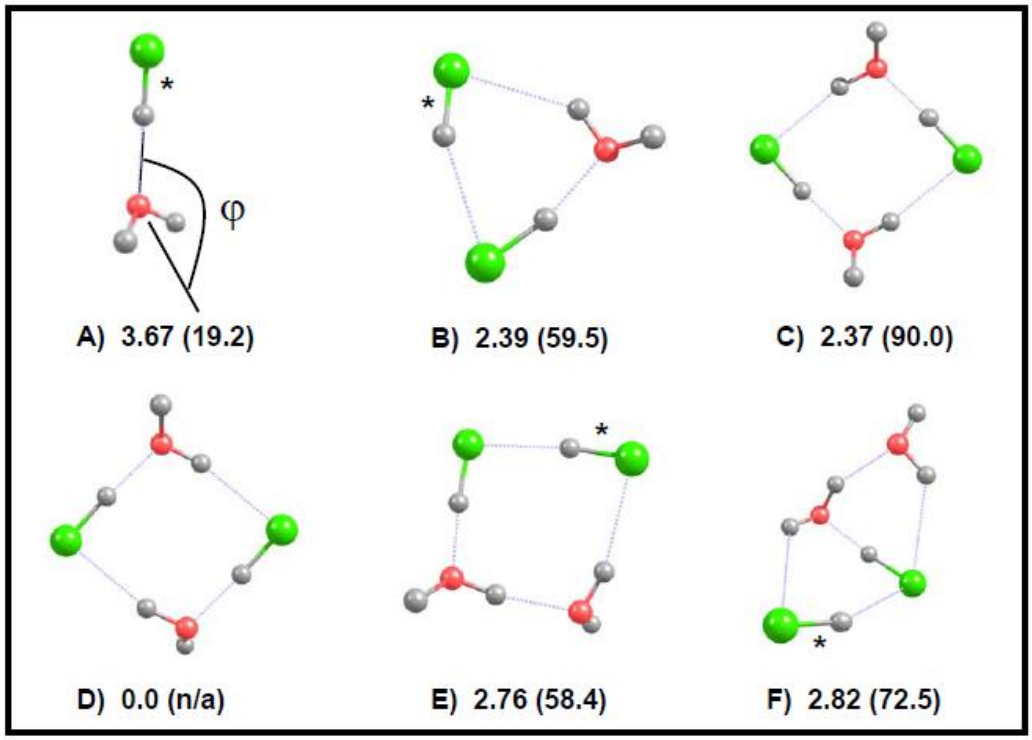

Figure 1.1 Illustration of HCl-Water Clusters. Illustration of HCl-Water Clusters. Illustrations of the structures of the mixed HCl-H_2O clusters that contribute to the bands, shown in Figure 4.1. The structures are calculated at the MP2/6-311+g(df,dp) level of theory. The asterisk represents the stretch in question. The numbers to the right of each label are the dipole moments, followed by the vibrational transition moment angle (VTMA) in parenthesis.

There is now a vast literature on the experimental and theoretical characterization of the acid dissociation mechanism. Molecular dynamics simulations employing various methodologies have led to a better understanding of the acid dissociation process in bulk water[18] and on ice surfaces.[19] Figure 1.1 shows a collection of the lowest energy isomers for small HCl water clusters, including the F) that shows the lowest energy ion separated pair. Infrared spectra of HCl on the surface of bulk ice and ice nanoparticles have provided important insights into the temperature dependence of acid ionization in environments relevant to the stratosphere and the chemistry associated with ozone depletion.[19a, 19b, 20] For the smaller $(HCl)_m(H_2O)_n$ clusters, there are many reports of

electronic structure calculations, which aim to determine the onset of acid ionization.[21] These *ab initio* studies generally agree that four water molecules are necessary before the ion pair becomes the minimum energy structure.[21b, 21c, 21e, 21f, 22] On the experimental front, microwave[22b, 23] and cavity ring-down infrared[24] spectroscopy have provided structural data for some of the smaller, undissociated $(HCl)_m(H_2O)_n$ clusters, such as the 1:1 and 1:2 complexes. Fourier transform infrared (FTIR) spectroscopy of these clusters grown in solid matrices[25] or formed in free-jet expansions[21j, 26] have provided overview spectra in the OH and HCl stretch regions. More recently, infrared spectra of $(HCl)_m(H_2O)_n$ clusters grown in helium nanodroplets were reported in the OH stretch[27] and HCl stretch[28,39] regions.

Infrared spectroscopy is particularly well suited to explore the structural properties of these clusters with increasing solvation, given that the HCl chromophore is a sensitive messenger of the dissociation process. Indeed, as the acid dissociates, the HCl stretch vibration should disappear, being replaced by the OH stretch vibrations of a protonated water moiety. Nevertheless, the infrared spectra of these cluster systems can be difficult to interpret, given the diversity of cluster sizes and isomeric structures produced in these environments. As the concentration increases, this distribution leads to broad spectral features that span several hundred wavenumbers and obscure the signatures of individual clusters, including those that may be stabilized as ion pairs. In the FTIR spectra of the free-jet, several sharp bands in the HCl stretch region are superimposed on a broad background that spans ~300 cm^{-1}.[21j, 26] The sharp bands were assigned to the HCl stretch transitions of smaller, undissociated $(HCl)_m(H_2O)_n$ clusters, and on the basis of isotopic substitution,[20d] the broad background was assigned to larger

undissociated clusters. The broad background in the FTIR gas phase spectra is similarly observed in the spectra obtained in solid matrices,[25] on the surface of ice films and nanoparticles, [19a, 19b, 20] and in helium nanodroplets.[29] In addition to the larger undissociated clusters, bands from dissociated ion pair clusters are also believed to contribute to these broad features. The origin and interpretation of the broad bands observed in these infrared spectra has been reviewed and discussed in a recent communication.[29]

A very recent helium nanodroplet study claimed the identification of a sharp spectral feature associated with the solvent separated $H_3O^+(H_2O)_3Cl^-$ species.[28] Given this intriguing result, it is timely to revisit the HCl stretch spectra of these species isolated in helium nanodroplets. Here, we have employed additional tools available to this method to arrive at unambiguous structural assignments of several bands that are common to both the gas phase and helium nanodroplet spectra, including the band previously assigned to the $H_3O^+(H_2O)_3Cl^-$ species.[30]

Ne-H_2O

A molecular level description of water remains an active research goal in molecular physics.[31] In fact, in 2005, *Science* ran an article of the 100 biggest questions in science today, and among them was the question of the structure of bulk water.[32] The experimental and theoretical study of small, gas phase water clusters has played an important role in achieving this goal. These systems have proven to be useful guides for probing the cooperative effects in liquid water.[33,31,34] Indeed, the combined spectroscopic and theoretical study of the water dimer has resulted in a quantitative description of the dimer potential.[34,33,] Nevertheless, the cyclic structures of the first few neutral water

clusters (trimer-pentamer) and the global minima of the hexamer (cage) and octamer (cube) that were reported in gas phase spectroscopic studies do not correspond to representative networks that are found in either liquid water or ice.[33,35] Indeed, in the networks of the first few water rings (trimer-pentamer), every molecule acts as a *single* donor/acceptor to its nearest neighbors; these networks are quite different from the ones present in liquid water and ice, in which *every* molecule acts as both a double donor and a double acceptor to nearest neighbors.[33] These networks are usually present in higher lying isomers of small neutral water clusters, which so far have not been probed experimentally.

The pioneering work of the sequential pick-up of monomers to form water clusters inside low temperature helium droplets has shown that the unique cluster growth process that occurs in this low temperature environment can kinetically steer the water hexamer system to a local minimum on the associated potential surface.[31,33] We report a similar approach for accessing the higher lying isomers of small water clusters, which also employs the helium nanodroplet isolation method. In the earlier reported infrared spectra of water clusters grown in helium droplets, it was shown that beyond the dimer, non-polar, cyclic species are formed, at least up to the hexamer.[33] With zero point effects taken into account, simulations showed that the insertion of water molecules into the preformed cyclic trimer, tetramer, or pentamer lead barrierlessly to the next larger cyclic species.[33] With the exception of the hexamer, these cyclic structures represent the global minima on the corresponding $(H_2O)_n$ potential energy surfaces.[35] In the present study, one or two Ne atoms are added to the He droplets prior to water pick-up, which results in IR bands that indicate the presence of a higher lying "3+1" isomer of the water tetramer

formed by the attachment of a water molecule to a preformed trimer ring. The assignment of this higher lying isomer is justified by the pressure dependence of the observed IR bands, the frequency and intensity pattern from high-level electronic structure calculations, as well as the electric field dependence of the newly observed bands. These findings point towards a general approach for stabilizing higher energy isomers of small water clusters that possess the structural motifs that resemble the transient structures within the hydrogen bonding networks of liquid water.

References

1. Onnes, H. K., *Commun. Phys. Lab. Univ. Leiden* **1908,** *108* (3), 163-179.

2. Becker, E. W.; Klingelhofer, R.; Lohse, P., *Z Naturforsch Pt A* **1961,** *16* (11), 1259-1259.

3. Harms, J.; Toennies, J. P.; Knuth, E. L., *J. Chem. Phys.* **1997,** *106* (8), 3348-3357.

4. Choi, M. Y.; Douberly, G. E.; Falconer, T. M.; Lewis, W. K.; Lindsay, C. M.; Merritt, J. M.; Stiles, P. L.; Miller, R. E., *Int. Rev. Phys. Chem.* **2006,** *25* (1-2), 15-75.

5. Toennies, J. P.; Vilesov, A. F., *Angew. Chem. Int. Ed.* **2004,** *43* (20), 2622-2648.

6. Whittle, E., D. A. D., Pimentel, G.C., *J. Chem. Phys* **1954,** *22, 1943-1944*.

7. Gough, T. E., M. M., P. A. Rowntree, and G. Scoles, *J. Chem. Phys.* **1985,** *83*, 4958-4959.

8. Goyal, S.; Schutt, D. L.; Scoles, G., *Phys. Rev. Lett.* **1994,** *73* (18), 2512-2512.

9. Gough, T. E., D. G. K., and Scoles, G., *Chem. Phys. Lett.* **1983,** *97*, 155-160.

10. Goyal, S., G. N. R., D. L. Schutt, and G. Scoles, *J. Phys. Chem.* **1991,** *95*, 4186-4189.

11. Ehbrecht, M., and F. Huisken, J. P. C. A., *J. Phys. Chem. A* **1997,** *101*, 7768-7777.

12. Frochtenicht, R.; Toennies, J. P.; Vilesov, A., *Chem. Phys. Lett.* **1994,** *229*, 1-7.

13. Stienkemeier, F.; Lehmann, K. K., *J. Phys. B.* **2006,** *39* (8), R127-R166.

14. Callegari, C.; Lehmann, K. K.; Schmied, R.; Scoles, G., *J. Chem. Phys.* **2001,** *115* (22), 10090-10110.

15. Bondybey, V. E.; Beyer, M. K., *Int. Rev. Phys. Chem.* **2002,** *21* (2), 277-306

16. (a) Zonnevylle, M. C.; Geerlings, J. J. C.; Vansanten, R. A., *J. Catal.* **1994,** *148* 417-426; (b) Toennies, J. P.; Vilesov, A. F., *Annu. Rev. Phys. Chem.* **1998,** *49*, 1-41; (c) Hermann, K.; Bagus, P. S.; Bauschlicher Jr., C. W., *Phys. Rev. B* **1984,** *30* (12), 7313-7316.

17. Slipchenko, M. N.; Vilesov, A. F., *Chem. Phys. Lett.* **2005,** *412* (1-3), 176-183.

18. (a) Buch, V.; Sadlej, J.; Aytemiz-Uras, N.; Devlin, J. P., *J. Phys. Chem. A* **2002,** *106* (41), 9374-9389; (b) Vissers, G. W. M.; McCoy, A. B., *J. Phys. Chem. A* **2006,** *110* (18), 5978-5981

19. (a) Douberly, G. E.; Merritt, J. M.; Miller, R. E., *Phys. Chem. Chem. Phys.* **2005,** *7* (3), 463-468; (b) Kwon, Y.; Whaley, K. B., *J. Phys. Chem. Solids.* **2005,** *66* (8-9), 1516-1519; (c) Kwon, Y.; Whaley, K. B., *J. Low Temp. Phys.* **2005,** *140* (3-4), 227-240; (d) Walker, K. A.; Evans, C. J.; Suh, S. H. K.; Gerry, M. C. L.; Watson, J. K. G., *J. Mol. Spectrosc.* **2001,** *209* (2), 178-191.

20. (a) Packer, M. J.; Clary, D. C., *J. Phys. Chem.* **1995,** *99* (39), 14323-14333; (b) Paesani, F.; Gianturco, F. A.; Whaley, K. B., *J. Chem. Phys.* **2001,** *115* (22), 10225-10238; (c) Re, S.; Osamura, Y.; Suzuki, Y.; Schaefer, H. F., *J. Chem. Phys.* **1998,** *109*

(3), 973-977; (d) Huang, W.; Zhai, H. J.; Wang, L. S., *J. Am. Chem. Soc.* **2010,** *132* (12), 4344-4351; (e) Koszinowski, K.; Schroder, D.; Schwarz, H., *Organometallics* **2004,** *23* (5), 1132-1139; (f) Chaban, G. M.; Gerber, R. B.; Janda, K. C., *J. Phys. Chem. A* **2001,** *105* (36), 8323-8332; (g) Neukermans, S.; Veldeman, N.; Janssens, E.; Lievens, P.; Chen, Z.; Schleyer, P. V. R., *Eur. Phys. J. D* **2007,** *45* (2), 301-308; (h) Cabaleiro-Lago, E. M.; Hermida-Ramon, J. M.; Rodriguez-Otero, J., *J. Chem. Phys.* **2002,** *117* (7), 3160-3168; (i) Stiles, P. L.; Miller, R. E., *J. Phys. Chem. A* **2006,** *110* (17), 5620-5628; (j) Masia, M.; Forbert, H.; Marx, D., *J. Phys. Chem. A* **2007,** *111* (49), 12181-12191.

21. (a) Bacelo, D. E.; Binning, R. C.; Ishikawa, Y., *J. Phys. Chem. A* **1999,** *103* (24), 4631-4640; (b) Mitric, R.; Burgel, C.; Burda, J.; Bonacic-Koutecky, V.; Fantucci, P., *Eur. Phys. J. D* **2003,** *24* (1-3), 41-44.

22. (a) Lehmann, K. K., *J. Chem. Phys.* **2004,** *120* (2), 513-515; (b) Kisiel, Z.; Pietrewicz, B. A.; Desyatnyk, O.; Pszczolkowski, L.; Struniewicz, I.; Sadlej, J., *J. Chem. Phys.* **2003,** *119* (12), 5907-5917; (c) Lindinger, A.; Toennies, J. P.; Vilesov, A. F., *J. Chem. Phys.* **2004,** *121* (24), 12282-12292.

23. Glaspell, G.; Hassan, H. M. A.; Elzatahry, A.; Abdalsayed, V.; El-Shall, M. S., *Top. Catal.* **2008,** *47* (1-2), 22-31.

24. (a) Schmied, R.; Carcabal, P.; Dokter, A. M.; Lonij, V. P. A.; Lehmann, K. K.; Scoles, G., *J. Chem. Phys.* **2004,** *121* (6), 2701-2710; (b) Choi, M. Y.; Miller, R. E., *Phys. Chem. Chem. Phys.* **2005,** *7* (20), 3565-3573.

25. Reber, A. C.; Khanna, S. N.; Castleman, A. W., *J. Am. Chem. Soc.* **2007,** *129* (33), 10189-10194.

26. Yetter, R. A.; Risha, G. A.; Son, S. F., *Proceedings of the Combustion Institute* **2009,** *32*, 1819-1838.

27. Sullivan, K.; Young, G.; Zachariah, M. R., *Combust. and Flame* **2009,** *156* (2), 302-309.

28. Paesani, F.; Zillich, R.; Kwon, Y.; Whaley, K. B., *Abstr Pap Am Chem S* **2004,** *228*, U227-U227.

29. Nauta, K.; Miller, R. E., *Science* **2000,** *287* (5451), 293-295.

30. Kennedy, D.; Norman, C., S*cience* **2005,** *309* (5731), 75-75.

31. Burnham, C. J.; Xantheas, S. S.; Miller, M. A.; Applegate, B. E.; Miller, R. E., *J. Chem. Phys.* **2002,** *117* (3), 1109-1122.

32. Kang, D.; Dai, J.; Hou, Y.; Yuan, J., *J. Chem. Phys.* **2010,** *133* (1), 014302-014309.

33. Xantheas, S. S., *Philo. Mag. B.* **1996,** *73*, 107-112.

CHAPTER 2

EXPERIMENTAL

Droplet Formation

Helium droplets are formed in a free jet expansion, as reported by Becker in 1961,[2] where 99.9995% pure He, with a backing pressure of about 25 bar, is passed through a 5 micron hole into vacuum. The nozzle is cryogenically cooled by a closed cycle He refrigerator to temperatures of about 15 K. With these nozzle conditions, the average droplet size is approximately 4000 helium atoms.[36] The droplets form in the relatively high pressure region of the expansion.[4] Then they evaporatively cool as the pressure falls below the equilibrium vapor pressure of the droplets. In the case of the UGA HENDI instrument this free jet expansion leads to a continuous source of He droplets. The He does not liquefy in the nozzle, so it escapes the high pressure gas region through the aperture and aggregates into droplets. These droplets then evaporatively cool to about 0.37 K.[13]

The distribution of sizes and densities of He droplets depends heavily on the size of the aperture, which is limited by the pumping speed, the backing pressure of the He gas, and the temperature of the nozzle.[4] The ability to change the size of the droplets is effective in allowing us to optimize the droplet size to achieve the maximum signal for the molecule or cluster that is under investigation. Figure 2.1 presents the experimental apparatus used for the experiments presented in this thesis.

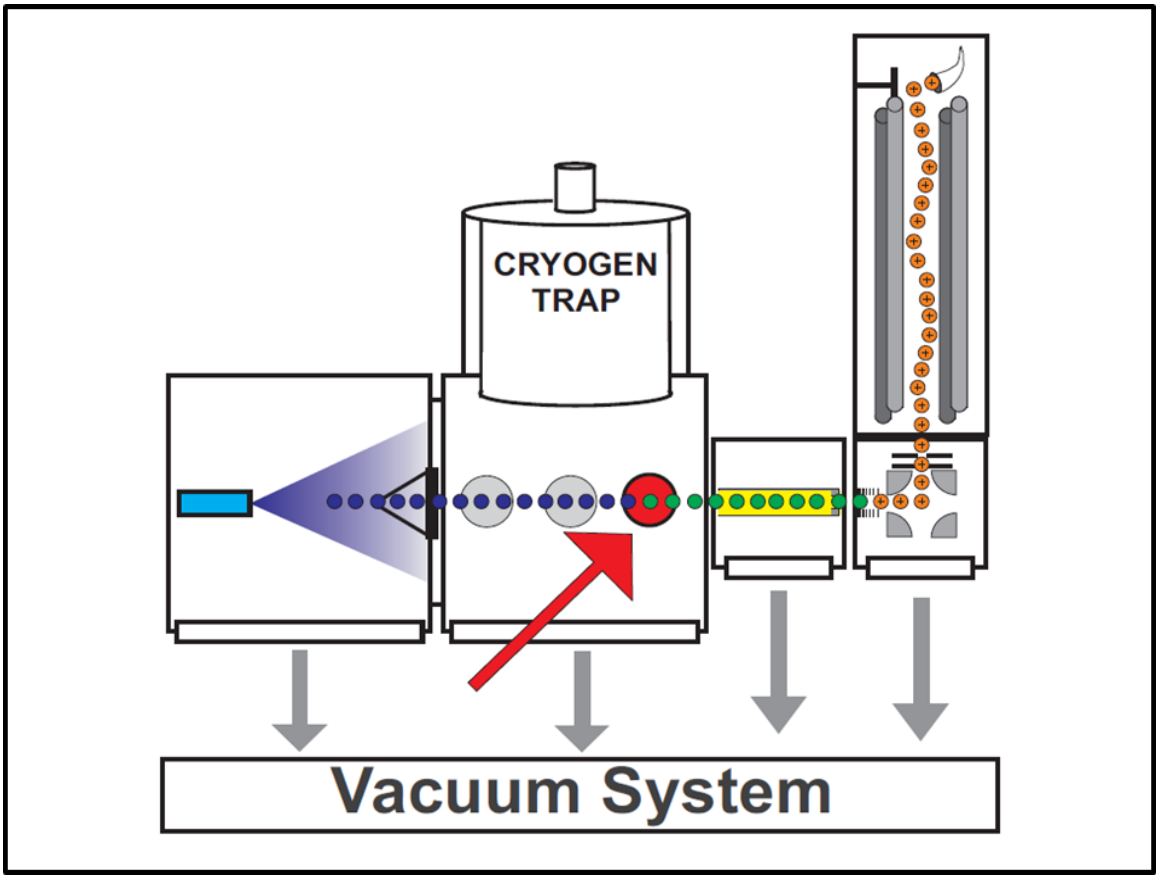

Figure 2.1 A Schematic of UGA HENDI Spectrometer. A schematic representation of the UGA HENDI spectrometer operated by the Douberly Lab.

As previously mentioned, the droplet size depends on the aperture size, the backing pressure, and the nozzle temperature.[14] About 1 cm downstream from the nozzle, the expansion is skimmed by a 0.4 mm diameter conical skimmer. The shape of the skimmer is extremely important as shockwaves may be created as the beam is skimmed.[15] A few cm downstream, dopants are "picked-up" as the droplet beam passes through a 2 cm long, differentially pumped gas cell, containing, for example, HCl and H_2O at a combined pressure of ~1.5 x 10^{-5} Torr.[4] In the case of the $(H_2O)_n$ Ne experiment, pick-up order is of the utmost importance. In the $(H_2O)_n$ Ne experiment, two pick up cells are used, one for each of the dopant species. To achieve the reliable pick up

of Ne first or second relative to water. Also by using two gas cells the pressures can be optimized for each individual dopant so that the average number of water or neon molecules/atoms can be properly estimated. The sequential pick-up of any species leads to the formation of clusters as the monomers rapidly condense within the droplet.[37] The condensation energy associated with this cluster formation is removed as the droplet evaporatively cools to 0.37 K.[38] A distribution of dopant cluster sizes is produced under these conditions.

Loading the Droplet

In order to perform spectroscopy using He nanodroplets one must dope the droplet with a molecule of interest. An advantage of using the HENDI technique is that only a minimal vapor pressure (about $1x10^{-5}$ torr) of the solute molecule is required. The pick-up technique is used to dope droplets in all of the studies presented in this thesis. The pick-up process occurs as an undoped droplet passes through a region of higher vapor pressure of the solute molecule. As the droplet travels through this region it will "pick-up" anything that it collides with. On the timescale of hundreds of picoseconds the excited molecule transfers its energy into the He droplet, which in turn releases that excess energy by evaporating He atoms away from the droplet.[14] Everything that gets picked up has some excess energy that is transferred into the droplet resulting in evaporated He atoms. This pick-up technique was first shown by Scoles and co-workers in 1985.[7]

The extent of doping of the droplet beam depends on the dopants' partial pressure. The process follows Poisson Statistics.[4] At a particular partial vapor pressure, the signal can be optimized to produce the desired species, whether it be a monomer, dimer, trimer,

etc. This can be predicted using the following equation for Poisson statistics in the form used to find the optimum pick up pressure.[4]

$$P_K = \frac{(\rho\sigma L)^k}{k!} e^{(-\rho\sigma L)}$$

Equation 2.1 Describes the pick-up process mathematically according to Poisson Statistics. The equation yields the relative pick up cell pressure (*P*) dependent on the average number of doped species (*k*) per droplet based upon the cross-sectional area of the droplet *(σ)*, the length of the pick-up cell (*L*), the gas density of dopant molecules *(ρ*).

Equation 2.1[4] describes the pick-up cell pressure, P, where *k* is the number of picked up species. The pick-up cell length is denoted by *L* and P_k is the pressure in the cell. The number density of the gas in the cell is denoted by ρ, and finally σ represents the crossectional area of the droplet.

Droplets and Their Role in Detection

The droplets are used for detection as well as containing and stabilizing a doped species. Just as excess energy is transferred to the droplet during a pick-up event, the energy of an absorbed photon of IR radiation is also transferred to the droplet. It only takes 5 cm^{-1} of energy to evaporate a He atom from a droplet.[12] Thus, if a doped molecule absorbs 3000 cm^{-1} it will couple that energy to the He droplet, which in turn sheds 600 He atoms. By losing that many He atoms, the droplet is now smaller in diameter than it was before its dopant was excited. Because the droplet diameter has been reduced that corresponds to an absorption event, it allows for the detection of the infrared spectrum in the following way. If the dopant is excited by IR radiation, the

excitation energy is released as the molecule's states are coupled to the droplet's. That energy is dissipated by evaporating the required number of He atoms for each absorption event.

Detection is achieved through the use of an Extrel quadrupole mass spectrometer.[39,40] Molecules must be ionized before being detected by the mass spectrometer. A smaller cross sectional area means that fewer droplets are ultimately ionized leading to a reduction in overall ion signal. This drop in mass spec ion intensity is the spectroscopic signal that is plotted *vs* wavelength to obtain a spectrum.[41]

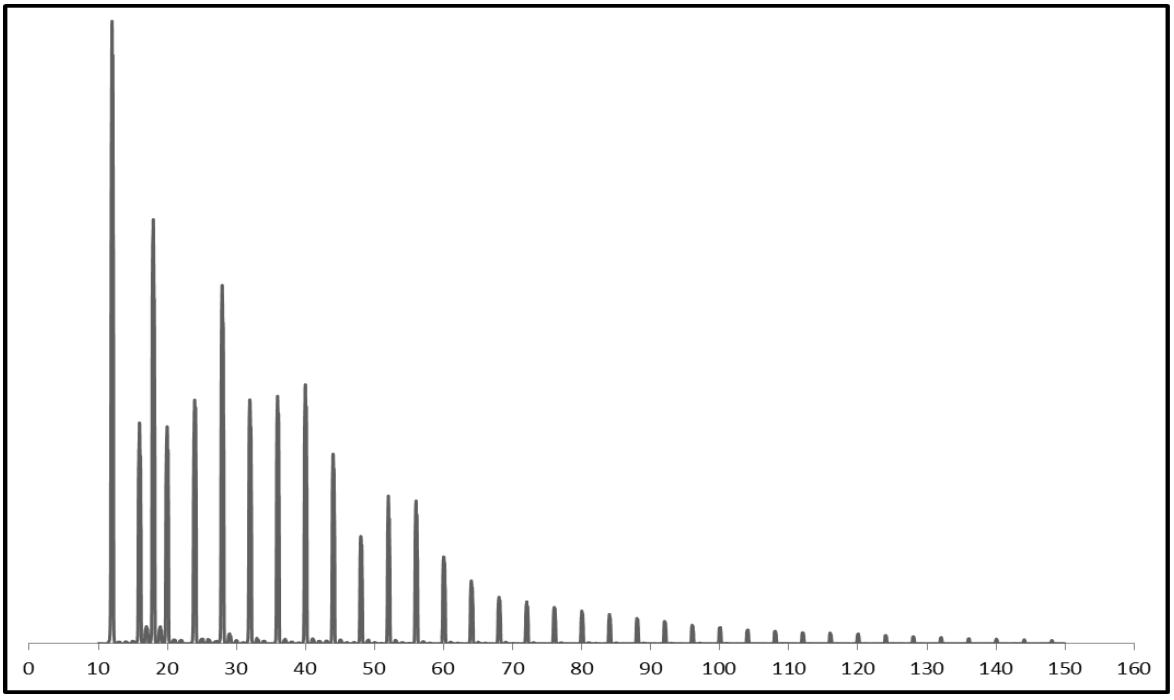

Figure 2.2 Mass Spectrum of He Beam Only. A mass spectrum of the He beam from 10 to 150 amu. The peaks occurring every 4 mass units are attributed to He_n^+ ions that form in the electron impact region of the mass spectrometer. Notice how there is an intensity decrease as the size of the ion increases.

A quadrupole mass spectrometer is used to measure the ion signal resulting from the electron impact ionization of the droplet beam. Upon electron impact, a He^+ ion is

produced in the droplet, which rapidly leads to the formation of $(He)_n^+$ cluster ions and the fragmentation of the droplet.[42] Alternatively, charge transfer[43] from He^+ to the solvated molecular cluster leads to the formation of $(HCl)_n^+$, $H^+(HCl)_n$, $H^+(H_2O)_n$, and $H^+(HCl)_m(H_2O)_n$ ions in the HCl-H_2O study. The mass spectrum of the beam with the above conditions is shown in Figure 2.2. It is very apparent upon looking at the mass spectrum that at every 4 amu there is a mass peak. Each of these peaks correspond to He^+ clusters that are formed as the droplet beam is ionized at 90 eV *via* electron bombardment. It is also clear that the intensities of these peaks, for the most part, follow a pattern where the most intense signal is at 4 amu and the intensities diminish as the mass increases.

Radiation Source

The idler beam output from a continuous wave (CW) infrared optical parametric oscillator (OPO) (Lockheed-Martin Aculight) overlaps the helium droplet beam in one of the following ways. First, the radiation may be sent counter propagating along the He beam path. This scanning method yields higher sensitivity than the second method because of the longer path length the laser and beam have when they are overlapped. In the second

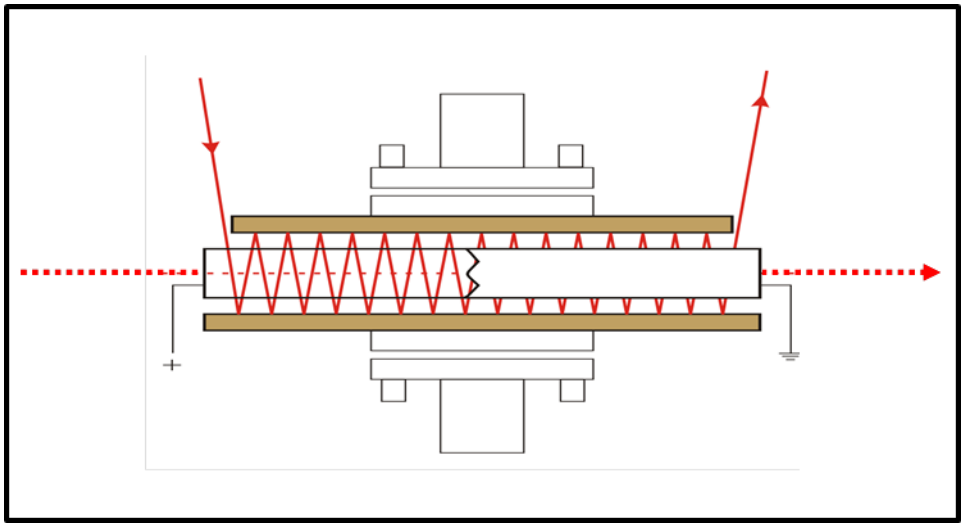

Figure 2.3 Multipass Stark Cell. Shows a schematic of the multipass Stark cell, used to apply a DC electric field to the area where the laser is bouncing back and forth between the mirrors to get maximum laser-droplet beam interaction. In this diagram the gold pieces represent mirrors, the red is the infrared beam path, and the electrodes are shown as white rectangles. The polarization of the light can be changed to align it parallel or perpendicular to the E field.

scanning method, a two-mirror multipass cell arrangement, as shown in Figure 2.3, can be used. The multipass cell is not as sensitive, but serves two purposes. First, the shorter (6 cm) path length ensures that cleaner droplets are probed that may be contaminated further down the instrument by background gas.[40] Second, with the addition of Stark electrodes perpendicular to the mirrors, only the area where an electric field is present is probed by the laser. By using this method, pendular state spectroscopy, where the molecule is aligned with the electric field based on its dipole moment, can be performed. In either case, the OPO output is amplitude modulated with a mechanical chopper at 171 Hz, and the ion signal is processed with a lock-in amplifier, which is referenced to the chopper frequency. Vibrational excitation of the helium solvated clusters leads to the evaporation of several hundred helium atoms (one atom for each 5 cm^{-1} of energy put in).[12] This loss of He atoms decreases the size of the He droplet's cross-sectional area.

As the droplets pass through the electron impact region of the mass spectrometer, a larger He droplet has a better chance of being ionized than a smaller droplet. Thus, when the laser is in resonance with a dopant's vibrational band the droplets are smaller and the ion signal being monitoring is decreased. Therefore, an infrared spectrum is acquired by monitoring this signal depletion as the OPO wavelength is tuned through the vibrational resonances of the solvated species. The tuning range of the OPO idler beam is from 2565 to 4000 cm^{-1} with an output power >1 W. A Glan-Taylor polarizer is used to attenuate this output in order to avoid saturation effects in the infrared spectra. A high precision wavemeter (Bristol Instruments 621A) is used for absolute and relative frequency calibration of the OPO idler wave.[40] The Douberly lab has devised an automated method to tune the laser by connecting the OPO module's tuning wrench to a stepper motor; an abbreviated description of how it works follows.[41] There are three ways to tune the laser, the first is translation of the crystal position with a wrench in the OPO module that shifts the output of the idler by one free spectral range of the intracavity etalon. This results in taking relatively large steps of about 13 cm^{-1}. The second way the OPO's idler beam can be tuned is through changing the etalon angle. This changes the amount of etalon material the light passes through as it resonates in the cavity. The etalon only allows one wavelength of light to build constructively. Therefore, changing the angle changes the wavelength of light of the idler beam. The third way the laser can be tuned is by changing the voltage applied to the piezo element of the seed laser. This allows for very fine tuning, allowing for a laser scanning resolution of roughly one thirty-thousandths of a cm^{-1}. In the following way the laser can be automatically and continuously tuned. First, the voltage on the piezo element is increased up to its maximum. This allows for

roughly 3 cm^{-1} of spectral coverage at high resolution. At the maximum piezo voltage the etalon hops up by about 3 cm^{-1}. The motor is automatically tuned with the stepper motor to maximize the overlap of the gain curve to give high, consistent

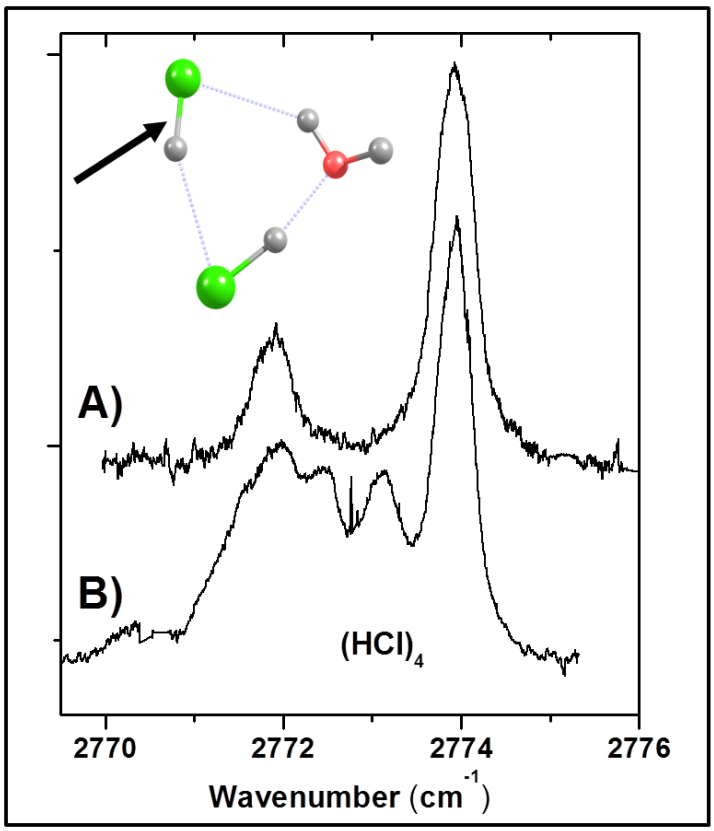

Figure 2.4 HCl-H_2O Spectra at 2774 cm^{-1}. Two spectra of HCl-H_2O clusters each scanned through the same region, but on different ion detection channels. Spectrum B was scanned on RF only mode, meaning all ions greater than 6 amu were allowed to pass the mass selector. Spectrum A was scanned on the mass 19 ion channel so only ions with mass of 19 amu were selected. By selecting the hydronium cation all spectroscopic signal from HCl only clusters was eliminated, as is the case with $(HCl)_4$, which is eliminated here.

power of the infrared beam. Then, instead of waiting for the piezo to scan back to zero and start scanning from 0V, the piezo element slowly scans down so that it covers the

spectral region missed by the etalon hop. In this way the laser is automatically tuned to cover some designated region in the mid IR.[41]

Two different schemes for detecting the ion signal attenuation are employed. Either the mass spectrometer is operated in the so-called "rf-only" mode, in which all masses greater than 6 amu are allowed to pass to the detector, or the dc voltage on the quadrupole is fixed to allow the transmission of a single mass/charge ratio peak. The latter detection scheme is used here, in both studies, to discriminate between the spectral signatures of different isotopomers or cluster sizes. The spectra in Figure 2.4 show how important and useful the ion channel selection can be. In the investigation of HCl-H_2O clusters the H-Cl stretches were probed with the laser. Because a distribution of clusters is formed as droplets pass through the pick-up cell, the spectroscopic signal of the HCl tetramer is in the middle of an important cluster band. When scanned with rf only mode spectroscopic signal could be seen from both components, but by switching the mass channel to focus on the hydronium cation, at a mass of 19 amu, all of the spectroscopic signal from HCl-only clusters were eliminated.

Optically Selected Mass Spectroscopy

Optically Selective Mass Spectra (OSMS) are obtained by scanning the quadrupole while the OPO frequency is fixed to the peak of a particular transition in the infrared spectrum.[44] An example of the OSMS technique is provided in the results of the HCl-H_2O investigation.[39] Since the OPO is amplitude modulated, the OSMS corresponds to the difference in the mass spectrum with and without the OPO present. In other words, the OSMS represents the mass spectrum of only those droplets that contain clusters that have been resonantly excited by the OPO. Furthermore, by employing the downstream

multipass cell excitation configuration, we significantly reduce the presence of OSMS artifact signals that arise from the pick-up of background molecules following vibrational excitation/relaxation.[40]

Stark Spectroscopy

Two parallel, stainless steel electrodes are positioned orthogonal to the multipass cell such that a static dc electric field can be applied to the laser/droplet beam interaction region. [17c] The electrodes are separated by 0.277(2) cm, and Stark field strengths up to ~60 kV/cm can be achieved. The calibration of the electrode spacing is described elsewhere.[45] A Fresnel Rhomb (II-VI Inc.) is used to align the polarization of the OPO idler wave either parallel or perpendicular to the applied Stark field. For the field dependence measurements, the OPO frequency is fixed to the peak of a particular band, and the applied Stark field is linearly ramped from zero-field to 55 kV/cm. For any one normal mode vibration, the vibrational transition moment angle (VTMA) is defined as the angle μ_p makes with the transition dipole moment vector (μ_t).[46]

Using the Gaussian 03 suite of programs,[47] we have computed (MP2 / 6-311+g(3df,3pd)) the harmonic vibrational frequencies, permanent dipole moments (μ_p) and vibrational transition moment angles (VTMAs) for the various isomers associated with the cluster sizes relevant to both studies presented in this thesis. The MP2 density matrix is used to obtain permanent dipole moments.

For a specific band in the infrared spectrum, the field ON to field OFF signal intensity ratio can be simulated, assuming a specific structure and value for the VTMA. In these simulations, the average projection of μ_t onto the OPO polarization axis is determined as a function of the Stark field strength. The weighting function for this

average is simply the normalized orientational distribution of μ_p about the lab-frame Stark field axis. This dipole distribution function, $P(\cos\theta)$, is computed according to the procedures of Kong and Bulthuis.[48] Here, θ is defined as the angle between μ_p and the Stark field axis. Calculations of $P(\cos\theta)$ assume the *ab initio* dipole moment components and rotational constants (divided by 3 to account for the helium solvent) for a specific cluster and a rotational temperature of 0.37 K. Projecting μ_t onto the polarization axis of the OPO (either parallel to or perpendicular to the Stark field axis) and averaging over θ gives the relative intensity due to cluster orientation at a given field strength,[49] where α is the VTMA:

$$A_{para}(\alpha) \propto \int_{-1}^{1} P(\cos\theta)[\sin^2\alpha + 2\cos^2\theta - 3\sin^2\alpha\cos^2\theta]d\cos\theta \qquad 2.2$$

and

$$A_{perp}(\alpha) \propto \int_{-1}^{1} P(\cos\theta)[2 - \sin^2\alpha - 2\cos^2\theta + 3\sin^2\alpha\cos^2\theta]d\cos\theta \qquad 2.3$$

For the simulations reported here, the field ON to field OFF intensity ratio is determined for Stark fields in the range of 0 to 50 kV/cm in increments of 5 kV/cm. This field dependence is determined for both polarization alignments. In the limit of infinite field, the asymptotic field dependence is due only to the VTMA (α), and is independent of μ_p (as long as μ_p is finite). For example, when α=0º, 54.75º and 90º (parallel polarization) the high field limit of the ON:OFF intensity ratios are 3, 1, and 0, respectively. However, the rate at which these asymptotic limits are approached depends strongly on the *magnitude* of μ_p. Hence, the field dependence of the ON:OFF intensity ratio is an

effective tool for assigning bands to specific isomers of $(HCl)_m(H_2O)_n$ clusters, since both μ_p and α are determined quite accurately at the MP2 level of theory used here.[46]

References

1. Becker, E. W.; Klingelhofer, R.; Lohse, P., *Z. Naturforsch Pt. A* **1961,** *16* (11), 1259-1259.

2. (a) Nauta, K.; Miller, R. E., *J. Chem. Phys.* **2000,** *113* (22), 10158-10168; (b) Reho, J. H.; Merker, U.; Radcliff, M. R.; Lehmann, K. K.; Scoles, G., *J. Phys. Chem. A* **2000,** *104* (16), 3620-3626.

3. Choi, M. Y.; Douberly, G. E.; Falconer, T. M.; Lewis, W. K.; Lindsay, C. M.; Merritt, J. M.; Stiles, P. L.; Miller, R. E., *Int. Rev. Phys. Chem.* **2006,** *25* (1-2), 15-75.

4. Frochtenicht, R.; Toennies, J. P.; Vilesov, A., *Chem. Phys. Lett.* **1994,** *229* (1-2), 1-7.

5. Stienkemeier, F.; Lehmann, K. K., *J. Phys. B* **2006,** *39* (8), R127-R166.

6. Callegari, C.; Lehmann, K. K.; Schmied, R.; Scoles, G., *J. Chem. Phys.* **2001,** *115* (22), 10090-10110.

7. Reho, J.; Higgins, J.; Callegari, C.; Lehmann, K. K.; Scoles, G., *J. Chem. Phys.* **2000,** *113* (21), 9686-9693.

8. Lindinger, A.; Neumark, D. M.; Toennies, J. P.; Vilesov, A. F., *Abstr Pap Am Chem S* **2000,** *220*, U209-U209.

9. Gough, T. E., M. M., Rowntree, P. E., and Scoles, G., *J. Chem. Phys.* **1985,** *83*, 4958-4962.

10. Brink, D. M.; Stringari, S., *Zeitschrift Fur Physik D* **1990,** *15* (3), 257-263.

11. Flynn, S. D.; Skvortsov, D.; Morrison, A. M.; Liang, T.; Choi, M. Y.; Douberly, G. E.; Vilesov, A. F., *J. Phys. Chem. Lett.* **2010,** (15), 2233-2238.

12. Morrison, A. M.; Flynn, S. D.; Liang, T.; Douberly, G. E., *J. Phys. Chem. A* **2010,** *114* (31), 8090-8098.

13. Morrison, A. M. Automation of an Aculight Optical Parametric Oscillator. University of Georgia, 2012.

14. Grebenev, S.; Lugovoi, E.; Sartakov, B. G.; Toennies, J. P.; Vilesov, A. F., *Faraday Discuss.* **2001,** *118*, 19-32.

15. Kwon, Y.; Whaley, K. B., *J. Chem. Phys.* **2001,** *115* (22), 10146-10153.

16. (a) Nauta, K.; Miller, R. E., *Chem. Phys. Lett.* **2001,** *350* (3-4), 225-232; (b) Lindinger, A.; Lugovoj, E.; Toennies, J. P.; Vilesov, A. F., *Z. Phys. Chem.* **2001,** *215*, 401-416.

17. Hermann, K.; Bagus, P. S.; Bauschlicher Jr., C. W., *Phys. Rev. B* **1984,** *30* (12), 7313-7316.

18. Hartmann, M.; Toennies, J. P.; Vilesov, A. F.; Benedek, G., Spectroscopic evidence for superfluidity in liquid He droplets. *Czeck. J. Phys.* **1996,** *46*, 2951-2956.

19. Grebenev, S.; Sartakov, B.; Toennies, J. P.; Vilesov, A., *Phys. Rev. Lett.* **2002,** *89* 22-30.

20. Toennies, J. P.; Vilesov, A. F.; Whaley, K. B., *Physics Today* **2001,** *54* (2), 31-37.

21. Yoon, B.; Hakkinen, H.; Landman, U., *J. Phys. Chem. A* **2003,** *107* (20), 4066-4071.

22. Stolcic, D.; Fischer, M.; Gantefor, G.; Kim, Y. D.; Sun, Q.; Jena, P., *J. Am. Chem. Soc.* **2003,** *125* (10), 2848-2849.

CHAPTER 3

NEON-WATER

Liquid helium droplets are formed in a continuous, cryogenic, nozzle expansion of helium gas into vacuum.[4,39] With the nozzle operated at 15 K, droplets are produced that contain ~10^4 He atoms on average. The droplets cool by evaporation to 0.4 K and are collimated into a beam using a conical skimmer.[38] This droplet beam subsequently passes through a differentially pumped "pick-up" chamber containing a variable pressure of water vapor (~10^{-7} to ~10^{-4} Torr).[39] As droplets traverse the pick-up zone, a statistical distribution of water capture events occurs, and the average number of water molecules introduced to each droplet is determined by the water pick-up cell pressure.[7] The interaction between individual water molecules is substantially larger than the interaction between each water and the helium solvent. Therefore, the sequential pick-up of multiple molecules leads exclusively to the formation of water clusters, and the condensation energy associated with this cluster formation is dissipated by helium evaporation.[43] Furthermore, the timescale between capture events is long enough (on the order of tens of microseconds) such that the internal energy of the cluster system is completely cooled to the droplet temperature prior to the addition of the next water molecule. The droplet sizes used here are sufficiently large to dissipate the condensation energy associated with the formation of water clusters well beyond the tetramer. The total condensation energy of the global minimum cyclic tetramer is computed to be approximately 10^4 cm^{-1}, which can be dissipated by the evaporation of ~2000 He atoms (5 cm^{-1} per atom).[12] Neon atoms

are added to the droplets either before or after the water by placing a second pick-up cell either upstream or downstream from the water cell. A tunable, narrow linewidth, IR optical parametric oscillator (OPO) is used to vibrationally excite the helium solvated molecular clusters. Vibrational excitation followed by relaxation results in the further reduction of the mean droplet size, which is detected as a decrease in the total ion signal, which originates from the electron impact ionization of the droplet beam. IR spectra are obtained by modulating the laser and processing the ion signal with a lock-in amplifier as the IR wavelength is tuned from 3150 to 3800 cm^{-1}.

Given the low temperature of the helium droplet (0.4 K), the rotational energy of the solvated water cluster is small enough such that its permanent electric dipole moment (μ_p) can be oriented in the laboratory frame with a modest externally applied electric field (<50 kV/cm).[4,50,51,25b] This electric field is applied to electrodes that are oriented orthogonal to a laser multipass cell (which defines the laser, droplet beam interaction region). By orienting the molecule in the lab frame, the intensity of vibrational bands can be studied with different laser polarizations, providing the angles between the vibrational transition moment vectors ($\boldsymbol{\mu_t}$) and the molecule's permanent dipole moment vector ($\boldsymbol{\mu_p}$). These angles are called vibrational transition moment angles (VTMA's).[25b,52] This measurement is the helium droplet analog to condensed phase linear dichroism spectroscopy. Furthermore, by measuring the vibrational band intensities as a function of the electric field strength, the magnitude of the permanent dipole moment can be obtained. Both the VTMA and $|\boldsymbol{\mu_p}|$ can be compared directly to *ab initio* quantum chemistry calculations of the various cluster species, resulting in a structural assignment tool that is in addition to the measured vibrational frequency pattern.

Results and Discussion

The sequential pick-up of water molecules by helium droplets leads to the IR spectrum shown in Figure 3.1a. The water pick-up cell pressure is adjusted such that, on average, four water molecules are picked-up by each droplet. Nevertheless, a statistical

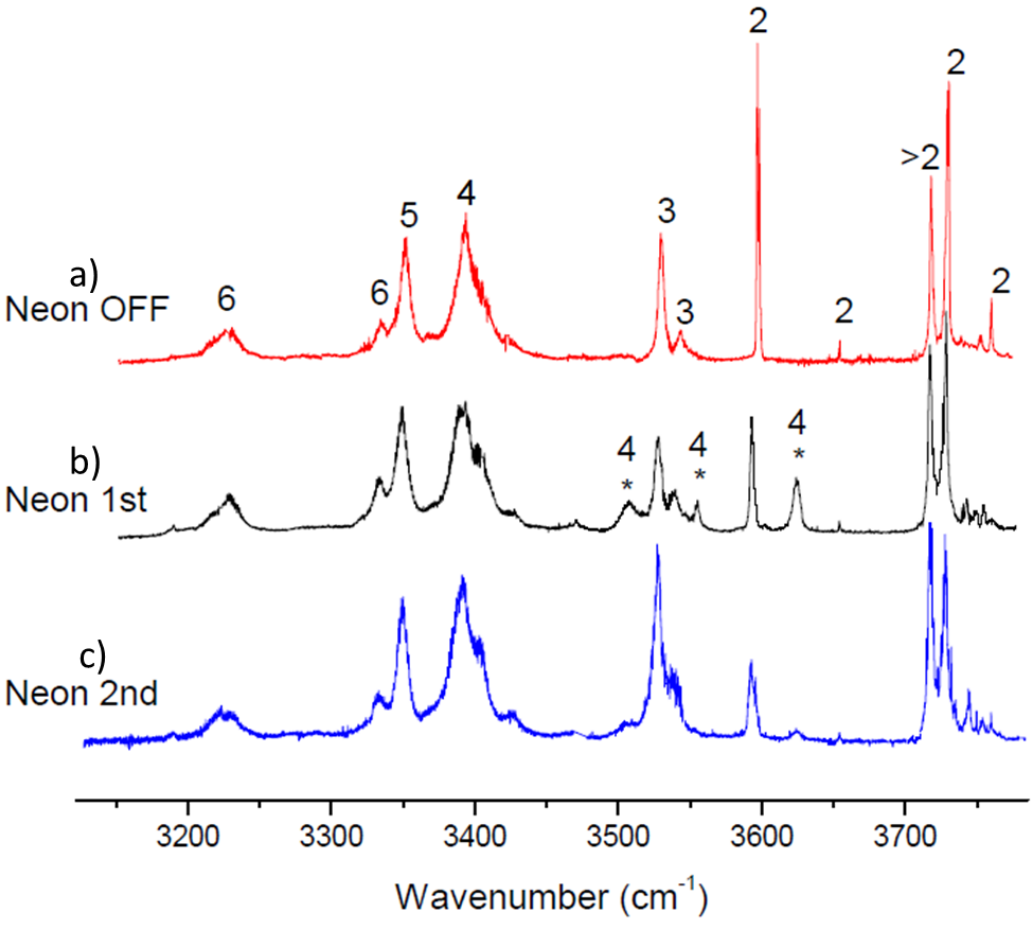

Figure 3.1 Ne-Water Experimental Spectra with Varying Pick-Up Order. The experimentally obtained spectra in this figure are of a) the water only spectrum, b) the pick up order is neon then water, c) the pickup order is water followed by neon. In Figure 3.1a) and 3.1b) the numbers correspond to the number of water molecules in each structure responsible for the band in the spectra. Figure 3.1b) uses an asterisk to denote a new peak due to some water neon complexes containing four water molecules each.

distribution of cluster sizes is formed, and bands associated with clusters up to the hexamer are observed. The numerical labels on the spectrum indicate the previously

assigned cluster size associated with each band. The spectrum in Figure 3.1b was obtained with similar water pick-up cell conditions. However, approximately 10^{-6} Torr of Ne gas was added to a 2 cm long pick-up cell, which is located upstream from the water pick-up cell. With these conditions, droplets contain, on average, one Ne atom before entering the water pick-up cell. The presence of single Ne atoms in the droplets prior to water cluster formation leads to new bands in the IR spectrum, denoted by an asterisk in Figure 3.1b). In addition to the features observed in the neat water spectrum, additional bands are observed in the 3450 - 3650 cm^{-1} region, which corresponds to the general enrgy of the hydrogen bonded OH stretching vibrations of the water dimer and trimer. It is interesting to note that the new spectral features are not observed in the spectrum obtained with the reverse pick-up order, that is, picking up the Neon atom second (see Figure 3.1c)).

Another observation from the experimental spectra in Figure 3.1 is the formation of a water dimer or trimer in the presence of a Ne atom leads to redshifts of the hydrogen bonded OH stretch bands by approximately 2 - 4 cm^{-1}. This small shift can be observed in the comparison of Figures 3.1a) with 3.1b). The new bands are more than four cm^{-1} away from the dimer or trimer bands. Therefore, the qualitatively new features in the spectrum upon sequential addition of water molecules to droplets containing a Ne atom are not simply due to shifts in the dimer and trimer bands.

In addition, each of the new bands, in Figure 3.1b) marked with an asterisk, at 3506, 3555, and 3624 cm^{-1} can be assigned a water cluster size by measuring the variation of each band's

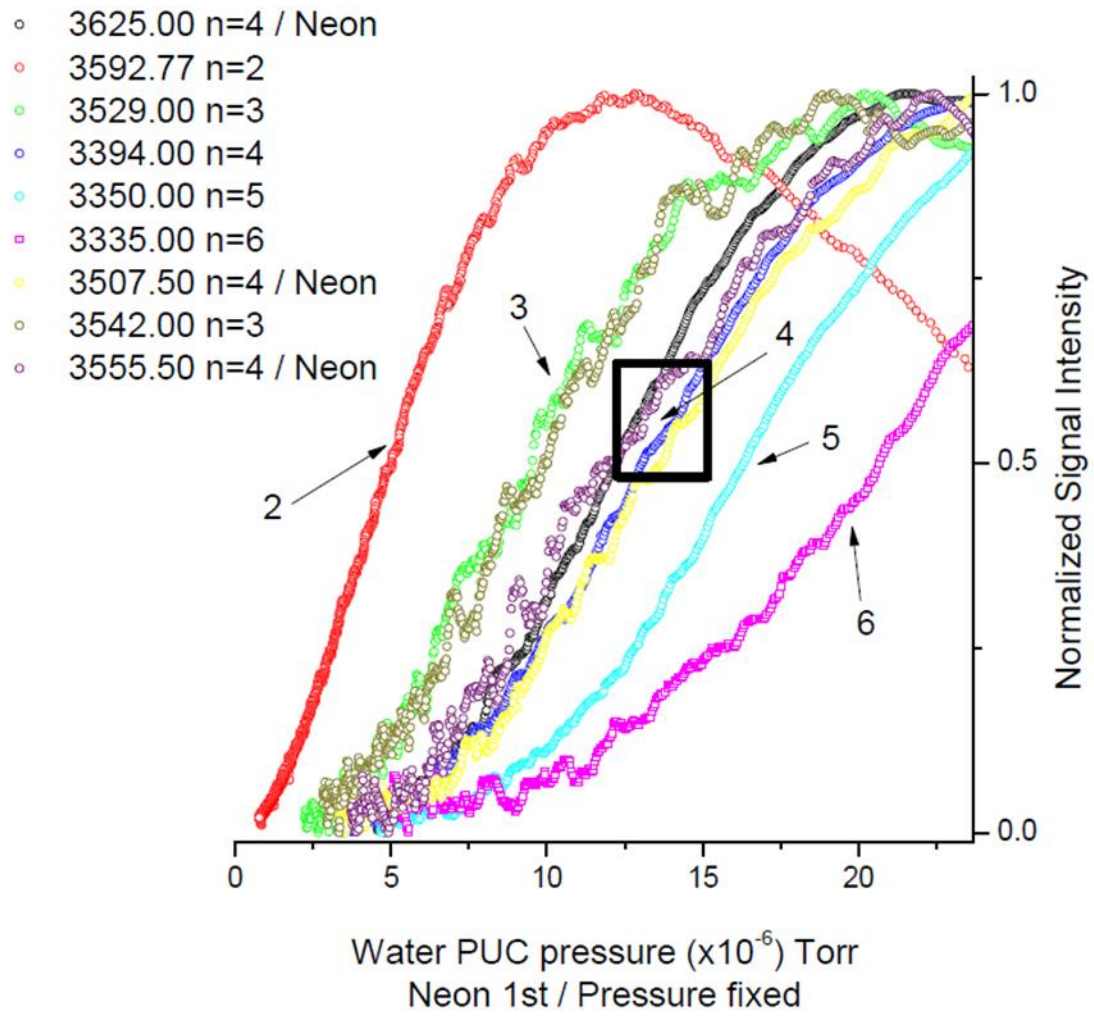

Figure 3.2 Pick-Up Cell Dependence Study at 3395 cm^{-1}. A group of plots showing the pick-up cell pressure dependence on signal intensity. By using the slope of the leading edge of each curve the number of water and neon molecules/atoms present in the structure responsible for each band can be obtained. Note the black, purple, blue, and yellow plots have a similar leading edge slope and all of them correspond to structures with 4 water molecules. The three new bands all result from a structure containing one Ne atom and four H_2O molecules in its structure.

signal intensity as the pressure is changed in the water pick-up cell. Figure 3.2 shows the pick-up cell pressure dependence curves for each band in Figure 3.1b. The curves associated with the new bands most closely match the pressure dependence of the cyclic tetramer band at 3395 cm^{-1}. In comparison, bands associated with the cyclic trimer and

pentamer grow in at lower and higher water pressures, respectively. This provides strong evidence for an assignment of the new features to $(H_2O)_4$–Ne clusters containing four water molecules.

Given the apparent formation of additional water tetramer clusters in droplets containing single Ne atoms, additional isomers on the $(H_2O)_4$ potential surface that would be consistent with the observed spectrum was considered. In addition to the cyclic tetramer global minimum, three locally stable isomers are found, which are labeled as 3+1A, 3+1B, and cage, as shown in Figure 3.3. The relative energetics of the n=4 isomers

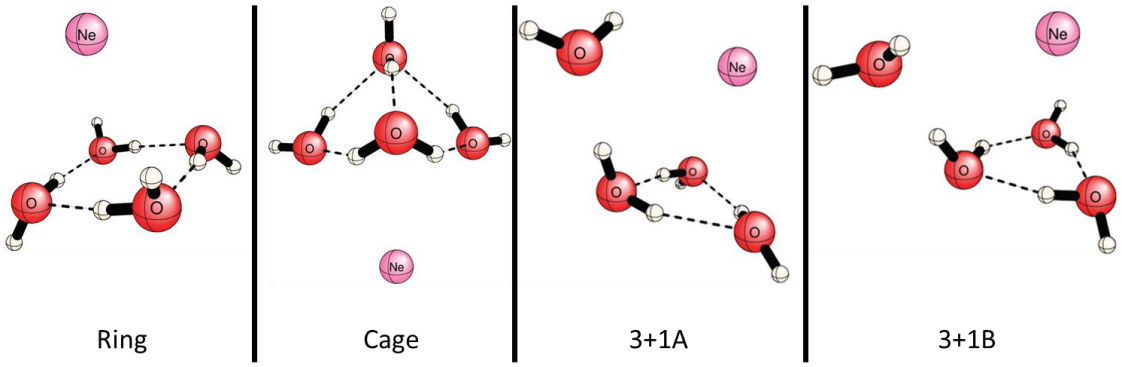

Figure 3.3 Stable Structures of Water Tetramer. Four locally stable isomers of Ne-$(H_2O)_4$ are shown here. The relative energetics of the structures can be seen in Table 3.1. Structures are based on calculations at the CCSD(T) level of theory. Energetics have also been calculated at the MP2 level and are present in Table 3.1 also.

are given in Table 3.1 at both the MP2 and CCSD(T) levels of theory. With the inclusion of anharmonic zero-point energy (ZPE), the MP2 electronic energies of the

$(H_2O)_4$		ΔE_{elec} [a]	ΔE_0 (harm ZPE)	ΔE_0 (anh ZPE)
MP2/avdz	cyclic (udud)	0.00	0.00	0.00
	3+1A: uud-w	6.93	5.71	5.45
	3+1B: udd-w	7.28	6.53	6.37
	Cage	4.85	4.35	4.12
CCSD(T)/avdz	cyclic (udud)	0.00	0.00	0.00
	3+1A: uud-w	6.73	5.69	5.43
	3+1B: udd-w	6.65	5.64	5.47
	Cage	-	-	-
$(H_2O)_4$—Ne				
MP2/avdz	cyclic (udud)	0.00	0.00	0.00
	3+1A: uud-w	6.75	5.65	5.54
	3+1B: udd-w	6.80	5.70	5.46
	Cage	5.29	4.47	3.27
CCSD(T)/avdz	cyclic (udud)	-	-	-
	3+1A: uud-w	-	-	-
	3+1B: udd-w	-	-	-
	Cage	-	-	-
$(H_2O)_4$—Ne		**μ** (Debye)		
MP2/avdz	cyclic (udud)	0.02		
	3+1A: uud-w	1.69		
	3+1B: udd-w	3.14		
	Cage	2.64		

a) Units are in kcal/mol, unless specified otherwise.

Table 3.1 *Ab initio* Energetics of Water Tetramers. Ab initio energetics of $(H_2O)_4$ and $(H_2O)_4$-Ne isomers.

cage, 3+1A and 3+1B isomers are found to be approximately 4.12, 5.45, and 6.37 kcal/mol higher than the cyclic global minimum, respectively. At this level of theory, the re-optimization of the structures in the presence of a single Ne atom only slightly shifts the relative energetics to 3.27, 5.54, and 5.46 kcal/mol, respectively. The (3+1)-Ne

isomers are nearly isoenergetic and consist of a cyclic trimer species in which one of the three ring waters (referred to as the acceptor-donor-donor water; ADD) acts as a hydrogen donor to the "dangling" water molecule.

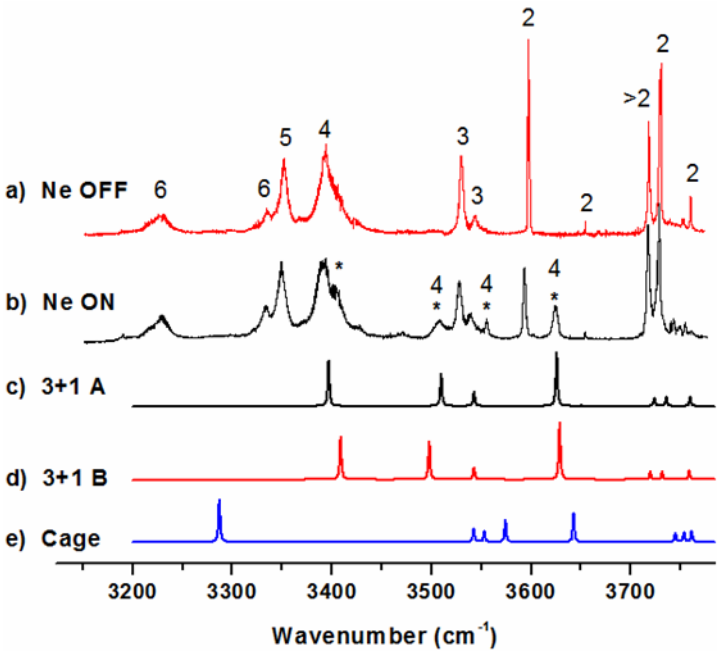

Figure 3.4 Ne-Water Spectra Both Theoretical and Experimental. Helium nanodroplet IR spectra of small water clusters assembled *via* the sequential pick up of water molecules. The numbers indicate the water cluster size as determined by the pick-up cell pressure dependence studies (see Figure 3.2), and the asterisks indicate new bands that appear upon introduction of a small amount of Ne to a pick-up cell positioned upstream from the water pick-up cell. a) Spectrum of neat water clusters inside helium nanodroplets. b) Spectrum obtained under similar conditions except that Ne is added to the upstream pick-up cell such that each droplet contains one Ne atom on average before passing into the water pick-up cell. c) Simulated 3+1A spectrum computed at the CCSD(T) / aug-cc-pVDZ level with the harmonic approximation. d) Simulated 3+1B spectrum at the same level of theory. e) Simulated cage isomer spectrum at the same level of theory. The harmonic frequencies are scaled by a factor of 0.964.

The CCSD(T) scaled harmonic frequency calculations for the three locally stable $(H_2O)_4$ isomers are shown in Figures 3.4 c-e. The patterns of predicted bands for the 3+1 isomers are in good agreement with the experimental bands assigned to $(H_2O)_4$–Ne clusters. However, a band predicted near 3290 cm^{-1} for the cage isomer is absent in the

droplet spectrum. In general, the agreement between experiment and theory is less satisfactory for the cage isomer. On the basis of MP2 frequency calculations for these systems, it is found that complexation of the $(H_2O)_4$ clusters with Ne leads only to relatively small frequency shifts, which justifies a direct comparison of the higher level CCSD(T) calculations of the neat clusters to the experimental spectra. CCSD(T) anharmonic frequency calculations were carried out for all of the locally stable $(H_2O)_4$ clusters and the global minimum ring isomer. It is useful to compare the experimental and anharmonic CCSD(T) frequency shifts ($\Delta\nu$) of the OH stretch bands relative to the degenerate hydrogen bonded ring vibrations of the ring tetramer. All of the frequency data, including these relative frequency shifts, are summarized in Table 3.2. There is

	MP2 / aug-cc-pVDZ / $(H_2O)_4$--Ne				CCSD(T) / aug-cc-pVDZ / $(H_2O)_4$				Experiment
	ω (cm^{-1})	Int (km/mol)	VTMA (°)	ν (cm^{-1})	ω (cm^{-1})	ω^* (cm^{-1})	ν (cm^{-1})	$\Delta\nu$ (cm^{-1}) [a]	$\Delta\nu$ (cm^{-1})
cyclic (udud)	3522	13	2.1	3257	3444	3320	3313	-57	--
	3486	1320	90.0	3317	3530	3403	3360	0	0
	3483	1325	90.0	3314	3530	3403	3360	0	0
3+1A: uud-w	3761	559	23.9	3581	3761	3626	3594	**234**	**229**
	3664	160	87.5	3499	3675	3543	3514	**154**	**160**
	3622	346	57.1	3456	3641	3510	3474	**114**	**111**
	3477	476	75.2	3322	3524	3397	3362	**2**	**7**
3+1B: udd-w	3763	595	19.6	3592	3765	3629	3581	**221**	**229**
	3663	131	68.2	3507	3675	3543	3510	**150**	**160**
	3612	399	81.1	3449	3629	3498	3460	**100**	**111**
	3488	443	59.4	3327	3536	3409	3376	**16**	**7**
cage	3792	311	90.0	3673	R	r	r	**260**	--
	3711	227	36.0	3538	R	r	r	**211**	--
	3695	95	89.9	3525	R	r	r	**198**	--
	3689	118	47.5	3564	R	r	r	**187**	--
	3392	495	12.4	3270	R	r	r	**-78**	--

n=4 ν_{exp} (cm^{-1})
3395
3402
3506
3555
3624

Table 3.2 Calculations of Vibrations for Various Water Structures. Ab initio harmonic (ω) and anharmonic (ν) frequencies, intensities and VTMAs.

overall excellent agreement between the 3+1A and 3+1B frequency shifts and the shifts observed experimentally, whereas there is qualitative disagreement for the cage isomer.

It is therefore reasonable to assign the newly observed $(H_2O)_4$–Ne spectral features to either one, or both, of the 3+1A, B isomers interacting with single Ne atoms. Specifically, the 3624 and 3555 cm^{-1} bands are assigned to asymmetric and symmetric OH stretching vibrations of the ADD water moiety, and the 3506 and 3402 cm^{-1} bands are assigned to the hydrogen bonded OH stretches of the AD ring waters. The free OH stretch region from 3710 to 3760 cm^{-1} is congested by bands due to the water dimer and larger clusters, and assigning bands in this region to specific, non-cyclic tetramer clusters is more difficult.

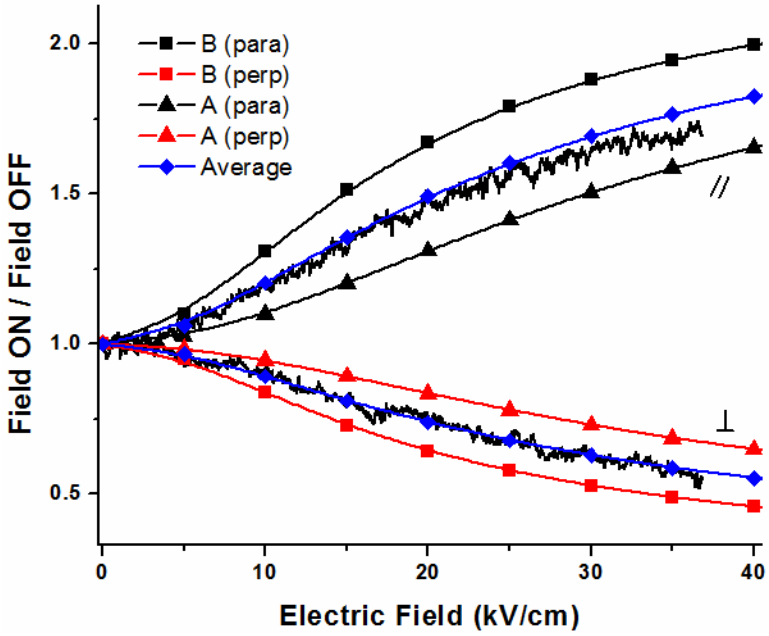

Figure 3.5 VTMA at 3625 cm^{-1} for Ne-Water. Electric field dependence of the peak signal intensity for the 3625 cm^{-1} band. The upward trending experimental curve (black) corresponds to the variation in signal intensity when the laser polarization is aligned parallel to the applied electric field. The downward trending curve is obtained with a perpendicular polarization alignment. Simulations are shown for the electric field dependence of the 3+1A-Ne isomer (▲) and the 3+1B-Ne isomer (■) for both the parallel (black) and perpendicular (red) polarization configurations. These simulations are generated using the dipole moments and rotational constants obtained from ab initio calculations (MP2/aug-cc-pVDZ), along with the computed VTMA for the non-ring H-bonded OH stretch of the ADD water moiety. The ab initio VTMAs used for the 3+1A-Ne and 3+1B-Ne simulations are 23.9 and 19.6 degrees, respectively. The simulated 3+1A-Ne and 3+1B-Ne curves are averaged to give the blue curves (◆).

The electric field dependence of the 3625 cm^{-1} band is shown in Figure 3.5, which provides further convincing support for the above assignments. With the laser electric field aligned parallel (perpendicular) to the applied Stark electric field, the signal intensity steadily grows (diminishes) as the Stark field is increased. This indicates that as the cluster's permanent dipole moment is oriented in the electric field, the vibrational transition dipole moment associated with the OH stretch is being brought into better (poorer) alignment with the laser electric field. These results definitively show that the cluster species responsible for the 3625 cm^{-1} band is polar and that the OH stretch vibration has an associated VTMA less than 54.5 degrees. The electric field dependences for the non-ring, hydrogen bonded OH stretches of the ADD water molecules in both 3+1 isomers are simulated using the MP2 dipole moments (1.69 (A), 3.14 (B) Debye) and VTMAs (23.9 (A), 19.6 (B) degrees) as input. The simulated curves for parallel and perpendicular laser polarization alignments bracket the experimental curves, and there is near quantitative agreement between the experimental curves and the simulated average effect for isomers A and B (blue curves).

In combination, the electric field measurements, pick-up cell pressure curves and anharmonic CCSD(T) frequency calculations provide strong evidence for the formation of non-cyclic 3+1 type water tetramers upon the sequential addition of four water molecules to droplets containing single Ne atoms. In addition to the formation of these non-cyclic tetramer clusters, a significant fraction of the droplet ensemble (~65% based on relative band intensities normalized to MP2 intensities) contains the global minimum

cyclic tetramer. Some of this cyclic population may be due to the fact that Ne pick-up is also statistical, leading to some droplets that do not contain Ne atoms.

In a previous theoretical study of water cluster growth, a flexible polarizable water potential (TTM2-F) was used to map the tetramer potential surface, and the cage and 3+1 isomers were found to be locally stable and separated from the cyclic minimum by approximately 70 cm^{-1} barriers.[33] These barrier heights were somewhat insensitive to zero-point energy (ZPE) effects. Using the tetramer potential surface, the long range, barrierless addition of water to a preformed cyclic trimer was characterized. For this study, it was assumed that, during the course of the $H_2O + (H_2O)_3 \rightarrow (H_2O)_4$ reaction, the system only travels downhill in potential energy and does not surmount barriers on the surface. With this assumption, the fractional yield of cyclic, 3+1 and cage tetramers is 0.76, 0.12 and 0.10, respectively. These conditions mimic somewhat the cluster growth in helium droplets, assuming the evaporative cooling is sufficiently fast to trap the system in local minima behind small barriers. However, the predicted barrier heights are rather small, and the higher energy $(H_2O)_4$ isomers are not observed in the neat helium droplet water spectrum. Apparently, as the fourth water molecule approaches a preformed cyclic trimer, the kinetic energy gain is incompletely quenched as the tetramer system moves to regions of lower potential energy, resulting in the exclusive formation of the cyclic global minimum.

The presence of a single Ne atom in the droplet significantly alters the final product distribution for the $H_2O + (H_2O)_3 \rightarrow (H_2O)_4$ reaction. This may simply be due to an enhanced barrier for the insertion of H_2O into the cyclic trimer when starting from the 3+1 “landing site”. Qualitatively, the reaction path can be visualized by interpolating the

internal coordinates between the 3+1B and ring tetramers, as shown in Figure 3.6. The location of the Ne atom in the optimized (3+1B)-Ne structure is positioned nominally along the 3+1B → ring reaction path. Hence, while the dimer and cyclic trimer are still formed barrierlessly, a possible explanation for the formation of non-cyclic tetramers is

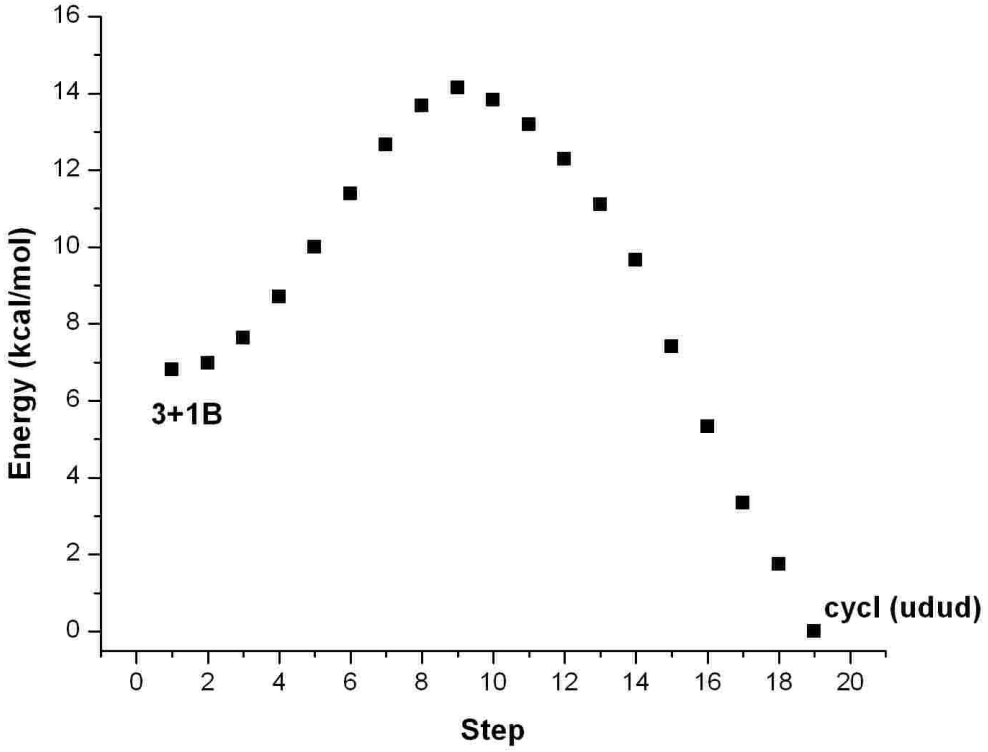

Figure 3.6 Energy of Calculated Optimization Points for 3+1B Water Structure. Interpolated z-matrix coordinates from 3+1B to ring. At each step, all of the degrees of freedom of the individual molecules (internal bond lengths and angles) are optimized (relaxed). An approximately 7 kcal/mol barrier is observed, which is unrealistic; but the insertion path is visualized somewhat, and it is qualitatively involves the motion of the +1 water through the nominal position of the Ne atom in the optimized (3+1B)-Ne cluster.

that ring insertion of the fourth water is sterically hindered by the Ne atom attached to the cyclic trimer. This is despite the fact that the interaction between the Ne atom and the cyclic trimer is computed to be relatively weak, namely 130 cm^{-1}. Apparently, the

insertion barrier in the mixed $(H_2O)_4$-Ne complex is sufficiently large such that the helium cooling is now capable of quenching the system prior to its rearrangement to the lower energy cyclic species.

Furthermore, for the long range addition of H_2O to a preformed trimer, it was shown that hydrogen bonds could be broken and reformed along downhill, barrierless paths leading directly to the cyclic tetramer, bypassing the 3+1 and cage landing sites. These channels are clearly still open when cluster growth occurs around a Ne atom, given that over half of the tetramer species are cyclic. Nevertheless, it is reasonable to suspect that the degree to which the cyclic species can be formed barrierlessly may also be altered by the presence of the Ne atom.

It is interesting to note that for the cage $\rightarrow$ ring reaction path, the location of the Ne atom in the optimized (cage)-Ne structure is positioned away from the ring insertion path, perhaps accounting for the absence of cage isomers in the IR spectrum.

Of course, much of this discussion is necessarily qualitative, and a quantitative description of the cluster growth process will require high level *ab initio* calculations of the tetramer potential surface, including the relevant barrier heights and the effect of the Neon and the evaporative helium cooling.

The presence of Ne in these water clusters is predicted to have at most a minor perturbation on their IR spectra and geometric structures. Therefore, this non-equilibrium, templated growth is indeed an effective means to probe non-cyclic water cluster structures, including those that resemble the open structural motifs present in liquid water. Further work is underway to determine if larger (n>4) open structures result from the sequential addition of water to $(H_2O)_4$-Ne clusters. Although the spectral

signatures of these species are likely to appear in the same region as the ADD hydrogen bonded stretches of the 3+1 structures, quasi-mass selective methods are being employed with HENDI laser spectroscopy to obtain the spectra of these larger clusters.

References

1. Choi, M. Y.; Douberly, G. E.; Falconer, T. M.; Lewis, W. K.; Lindsay, C. M.; Merritt, J. M.; Stiles, P. L.; Miller, R. E., *Int. Rev. Phys. Chem.* **2006,** *25* (1-2), 15-75.

2. Flynn, S. D.; Skvortsov, D.; Morrison, A. M.; Liang, T.; Choi, M. Y.; Douberly, G. E.; Vilesov, A. F., *J. Phys. Chem. Lett.* **2010,** (15), 2233-2238.

3. Lindinger, A.; Neumark, D. M.; Toennies, J. P.; Vilesov, A. F., *Abstr. Pap. Am. Chem. S.* **2000,** *220*, U209-U209.

4. Gough, T. E., M. M., Rowntree, P. A., and Scoles, G., *J. Chem. Phys.* **1985,** *83*, 4958-4962.

5. Kwon, Y.; Whaley, K. B., *J. Chem. Phys.* **2001,** *115* (22), 10146-10153.

6. Brink, D. M.; Stringari, S., *Z. Phys. D* **1990,** *15* (3), 257-263.

7. Dong, F.; Miller, R. E., *Science* **2002,** *298* (5596), 1227-1230.

8. Choi, M. Y.; Dong, F.; Miller, R. E., *Philos. Trans. R. Soc.f London Ser. a* **2005,** *363* (1827), 393-412.

9. Choi, M. Y.; Miller, R. E., *Phys. Chem. Chem. Phys.* **2005,** *7* (20), 3565-3573.

10. Choi, M. Y.; Dong, F.; Han, S. W.; Miller, R. E., *J. Phys. Chem. A* **2008,** *112* (31), 7185-7190.

11. Burnham, C. J.; Xantheas, S. S.; Miller, M. A.; Applegate, B. E.; Miller, R. E., *J. Chem. Phys.* **2002,** *117* (3), 1109-1122.

CHAPTER 4

HCl-WATER

Results and Discussion

The helium nanodroplet survey scan of the HCl stretch region is shown in Figure 4.1. The spectrum has several sharp features superimposed on a broad background signal that spans the 2570 to 2850 cm^{-1} region. Bands above 2750 cm^{-1} associated with pure HCl clusters (m=1-5)[53] are not present in this spectrum since the mass spectrometer is fixed to m/z=19 u (H_3O^+). The sharp bands observed here are assigned to the HCl stretches of mixed $(HCl)_m(H_2O)_n$ clusters with m=(1-3) and n=(1,2). The m:n assignments shown in the figure are based on the pick-up cell (PUC) pressure dependence of each band. The PUC dependence of the signal at 2580 and 2640 cm^{-1} indicates that the broad background arises from $(HCl)_m(H_2O)_n$ clusters with m>3 and n>2. As discussed below, the combination of harmonic frequency calculations, dipole moment measurements, and an analysis of the VTMAs leads to a firm confirmation of the PUC assignments and also provides structural assignments for each of the sharp bands.

In the previous FTIR "ragout" jet spectroscopic study of Fárník et. al.,[21j, 26] the HCl stretch region for mixed HCl-H_2O clusters was similarly shown to consist of several relatively sharp (~5-20 cm^{-1}) absorptions superimposed on a broad (~200 cm^{-1}) background absorption centered around 2550 cm^{-1}. The sharp features were also

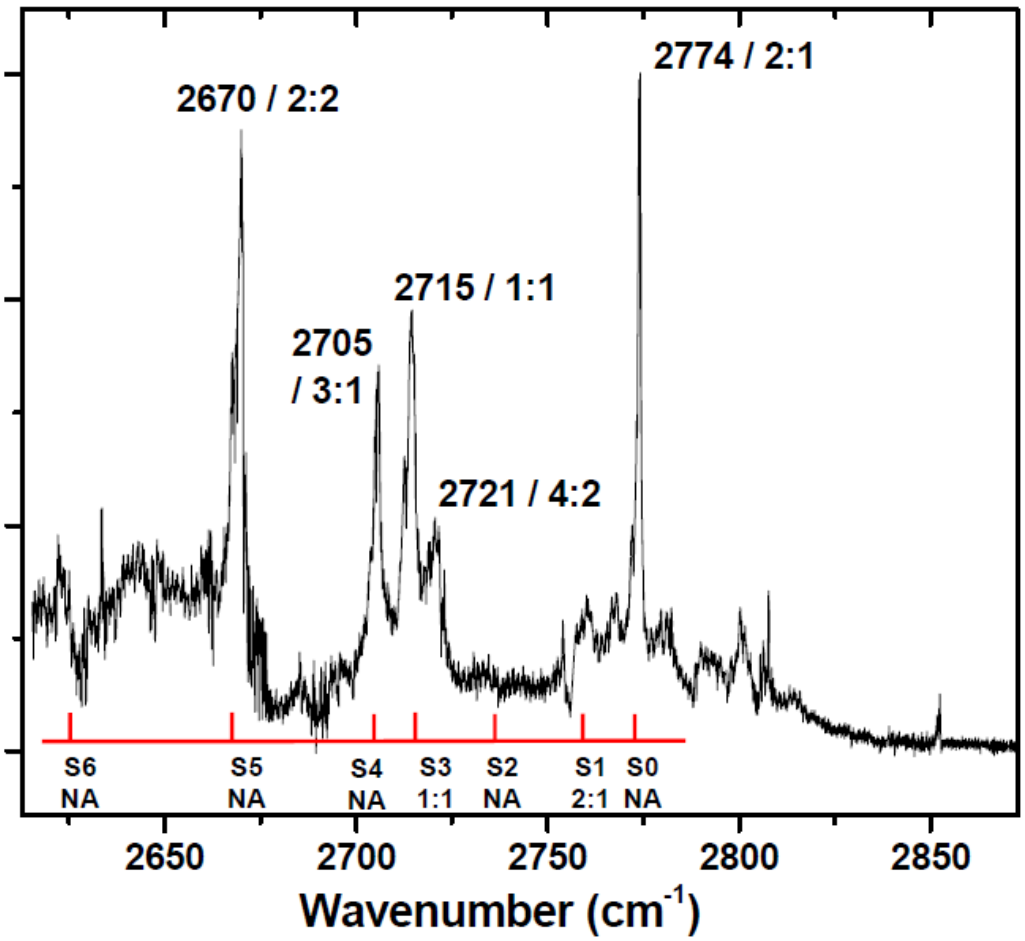

Figure 4.1 Broad Survey Scan of the H-Cl Stretch. A broad survey scan of the H-Cl stretch region. Appropriate ratios of HCl:H_2O and the center frequency of each band are provided at the maximum of each peak in the spectrum. The bands are labeled in order of energy from S0 through S6. Bands with a ratio below them have had their m:n ratio discerned already. The peaks with a NA at the bottom were not assigned before beginning this study.

assigned to HCl stretch bands of small mixed $(HCl)_m(H_2O)_n$ clusters. The authors speculated that the underlying broad feature was partially due to the $(H_3O)^+$ hydronium stretches of protolytically dissociated clusters. However, the broad feature was later assigned to larger undissociated mixed clusters on the basis of a 300 cm^{-1} redshift of the feature in the analogous $(HBr)_m(H_2O)_n$ spectrum.[20d] Furthermore, substituting D_2O for H_2O had no effect on the position of the broad adsorption.[20d] The position and

assignments of the sharp absorptions in the FTIR jet spectrum are shown along the bottom of Figure 4.1 (labels S0 to S6). Bands labeled as NA were not assigned at that time. In general, for the mixed cyclic complexes beyond the binary species, the higher frequency HCl stretches (those above ~2600 cm^{-1}) are associated with the HCl moieties that act as hydrogen donors to other HCl molecules. In comparison, the bands below 2600 cm^{-1} correspond to the stretching of HCl molecules that are hydrogen donors to H_2O. We denote these two distinct HCl stretches as Cl-H⋯Cl and Cl-H⋯O, respectively. An example of the latter type is the Cl-H⋯O stretch in the 1:2 complex, which was observed in the FTIR jet spectrum at 2460 cm^{-1}.[21j] We do not observe these Cl-H⋯O stretch bands of the 1:n (n>1) clusters given the tuning range of our OPO.

$\underline{(HCl)_1(H_2O)_1}$

The S3 band was previously assigned to the HCl stretch of the 1:1 complex in both the gas phase [21j, 24, 26] and in helium droplets,[54] and our PUC measurements are consistent with these assignments. Figure 4.2 shows our measurement of the S3 band using two

different mass spectrometer detection schemes. In Fig 4.2A, the detection channel is m/z=19 amu (H_3O^+), which results in two closely spaced bands separated by ~2 cm^{-1}. This splitting has been assigned to the $^{35}Cl/^{37}Cl$ isotopomers of the 1:1 complex,[54] which is consistent with the 2 cm^{-1} isotope splitting predicted by *ab initio* calculations. The presence of both peaks in the spectrum indicates that both isotopomers produce H_3O^+ ions upon fragmentation in the ionization region of the mass spectrometer. In contrast, when the mass spectrometer is fixed to m/z=36 amu (Fig. 4.2B), only the higher frequency band due to $(H^{35}Cl)(H_2O)$ is observed, indicating that the 36 u peak in the mass

spectrum is mainly associated with the $(H^{35}Cl)^+$ ion. Please note here that m/z=36 u also corresponds to $(He)_9^+$, which is formed upon ionization of droplets containing *both* isotopomers. As a result of this, the m/z=36 u channel is not completely specific to the $(H^{35}Cl)(H_2O)$ isotopomer, and a weak signal due to $(H^{37}Cl)(H_2O)$ is barely visible at 2712.75 cm^{-1}.

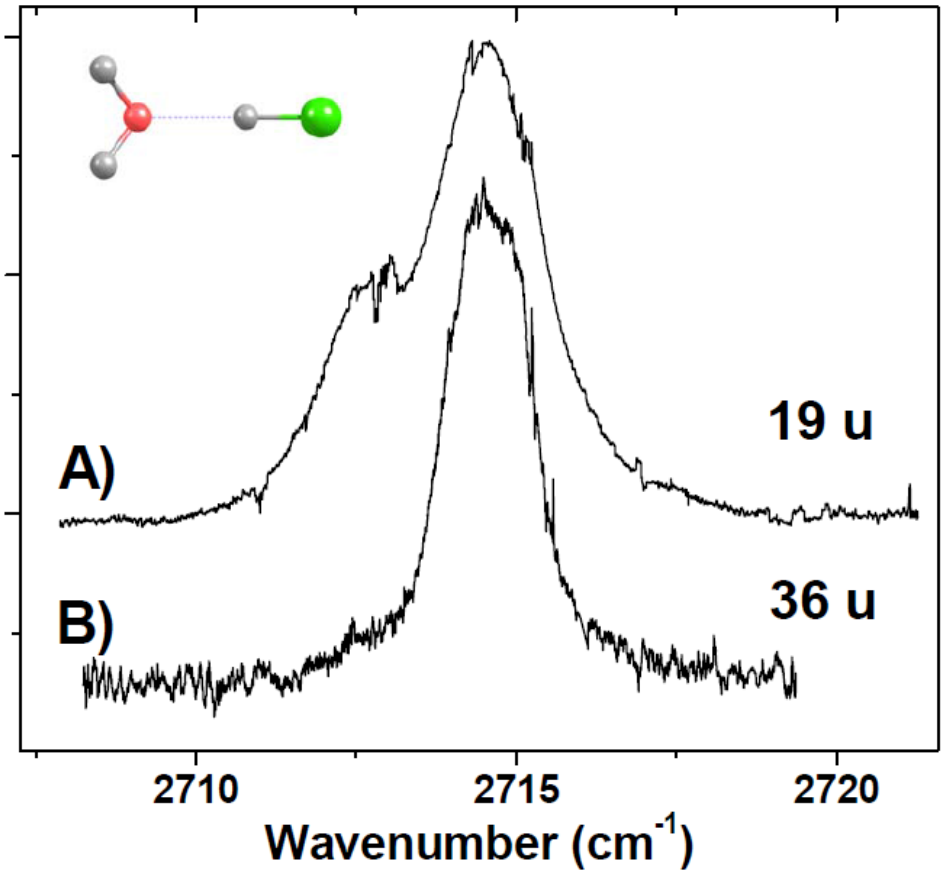

Figure 4.2 Comparison of Spectra Scanned on Various Mass Channels. Two spectra of the same region scanned on differing mass channels. When scanned on mass channel 36 amu, only ^{35}Cl isotopes are recognized by the mass spectrometer, this indicates that the higher frequency band is mostly from ^{37}Cl isotopes.

The HCl stretch band of $(H^{35}Cl)(H_2O)$ at 2714.6 cm^{-1} is redshifted 171 cm^{-1} from the HCl monomer band in helium droplets.[53-54] This large frequency shift is indicative of a structure in which the HCl acts as a hydrogen donor to H_2O. This redshift is 8.7 cm^{-1}

larger than that for the gas phase complex,[21j, 26] which agrees well with the previously established linear relationship between the complexation induced redshift and the solvent frequency shift due to the helium.[17c] Consistent with the magnitude of the redshift, the computed structure of the 1:1 complex has a C_s symmetry equilibrium geometry (φ=135º) with HCl acting as the hydrogen donor. Also, note that the linewidth of the ($H^{35}Cl$)(H_2O) band is 1.46 cm^{-1}, obscuring the rotational fine structure that would otherwise be observed for a cluster this size. This width is 10 times larger than observed in the high resolution gas phase spectrum, where the broadening was attributed to vibrational predissociation.[24] Apparently, the vibrational dynamics are accelerated due to interactions with the helium, as observed for other helium solvated hydrogen bonded clusters.[55]

Figure 4.3 shows the electric field dependence of the signal with the OPO frequency at 2714.3 cm^{-1} and the mass spectrometer tuned to m/z=36 u. For these measurements, the HCl and H_2O PUC pressures are reduced in order to eliminate signal contributions from the broad background due to larger clusters. When the OPO polarization is aligned parallel to the applied Stark field, the signal increases to over twice the zero-field level as the field increases beyond 40 kV/cm, whereas the signal is reduced to half the zero-field value with the perpendicular polarization configuration. These results are consistent with a vibration that has a VTMA close to zero.[17c] The circles in Figure 4.3 are the simulated field ON:OFF intensity ratios, assuming the C_s equilibrium structure of the HCl-H_2O complex (μ_a=3.46 D, α=19.2º, and A=11.5 cm^{-1}). Here, the red and blue points are for parallel and perpendicular polarization alignments, respectively.

The simulated field dependence for the C_s geometry is in rather poor agreement with the experiment, which can be understood by considering the double-well potential associated with the out of plane bending of the water molecule.[21i] For this potential, the transition state is C_{2v} (φ=180°), and the *ab initio* barrier between equivalent C_s (φ=135°) structures is approximately 65 cm^{-1}.[21i] The zero-point level was determined to be only a

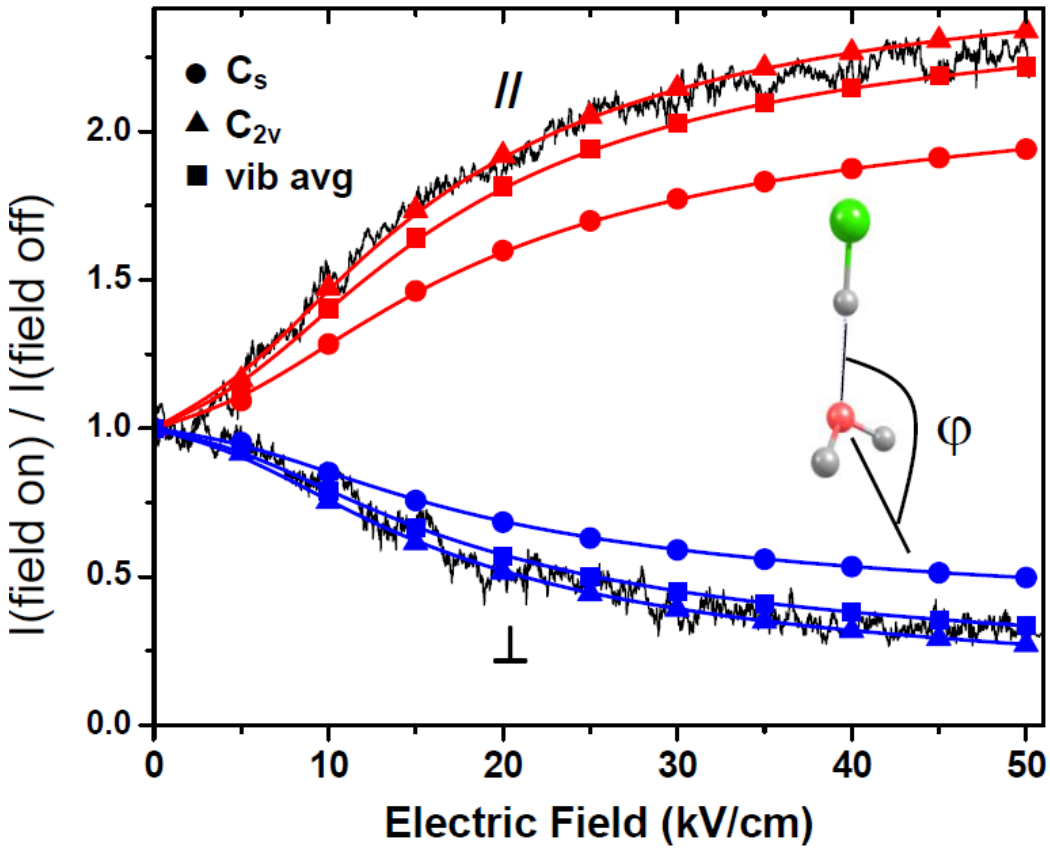

Figure 4.3 VTMA of HCl-H_2O cluster at 2714.3 cm^{-1}. A plot of the change in signal as the electric field between the Stark electrodes is ramped from 0 to 50 kV/cm with the laser maintained at 2714.3 cm^{-1}. When the light polarization matches the direction of the applied electric field the HCl-H_2O cluster signal increases with the increasing electric field. When the light is polarized perpendicular to the electric field the signal decreases as the field is increased. The blue lines are the predicted perpendicular field dependencies. The red lines represent the parallel field dependence also predicted at MP2/6-311+f(3df,3pd) level of theory. The circles are for the C_s symmetric cluster. The C_{2v} structure yields better results, and are represented as triangles. The squares represent the vibrational average of the two structures.

few cm^{-1} below the barrier. Consistent with these computations, gas phase studies in the microwave [23c] and the infrared [26] both conclude an *effective* C_{2v} structure at the zero-point level. In a recent helium droplet study of the asymmetric OH stretch,[56] transitions were observed from *both* K=0 and K=1 states, indicating the presence of two distinct nuclear spin species, consistent with a C_{2v} structure. Furthermore, the *A* rotational constant was determined to be >14 cm^{-1}, which can be compared to the C_s and C_{2v} *ab initio* values of 11.52 and 14.39 cm^{-1}, respectively. We have also simulated the field dependence assuming a C_{2v} structure for HCl-H_2O (μ_a=3.92 D, α=0.0º, and *A*=14.4 cm^{-1}) (triangles in Fig 4.3). In comparison to the C_s simulation, the agreement with experiment is substantially better for the C_{2v} case. From the ground state wavefunction in the double-well bending potential, we obtain expectation values of μ_a and α equal to 3.65 D and 13.0º, respectively. Simulations of the field dependence using these vibrationally averaged parameters are shown as squares in Figure 4.3. It is also interesting to note that the barrier height for the out of plane water bend should be *reduced* upon solvation in the helium droplet. This is apparent upon considering the dipole-induced polarization of the helium solvent, which reduces the free energy of the complex at all values of φ. However, this effect is maximized at the C_{2v} geometry, which in turn results in a reduction of the barrier height. According to a mean field approach used previously for the tunneling potential of $(HF)_2$,[57] helium solvation reduces the barrier between the two C_s minima by 9.2 cm^{-1} (see Figure 4.4), leading to a slightly more planar geometry with $\langle\mu_a\rangle$=3.71 D and $\langle\alpha\rangle$=11.4º.

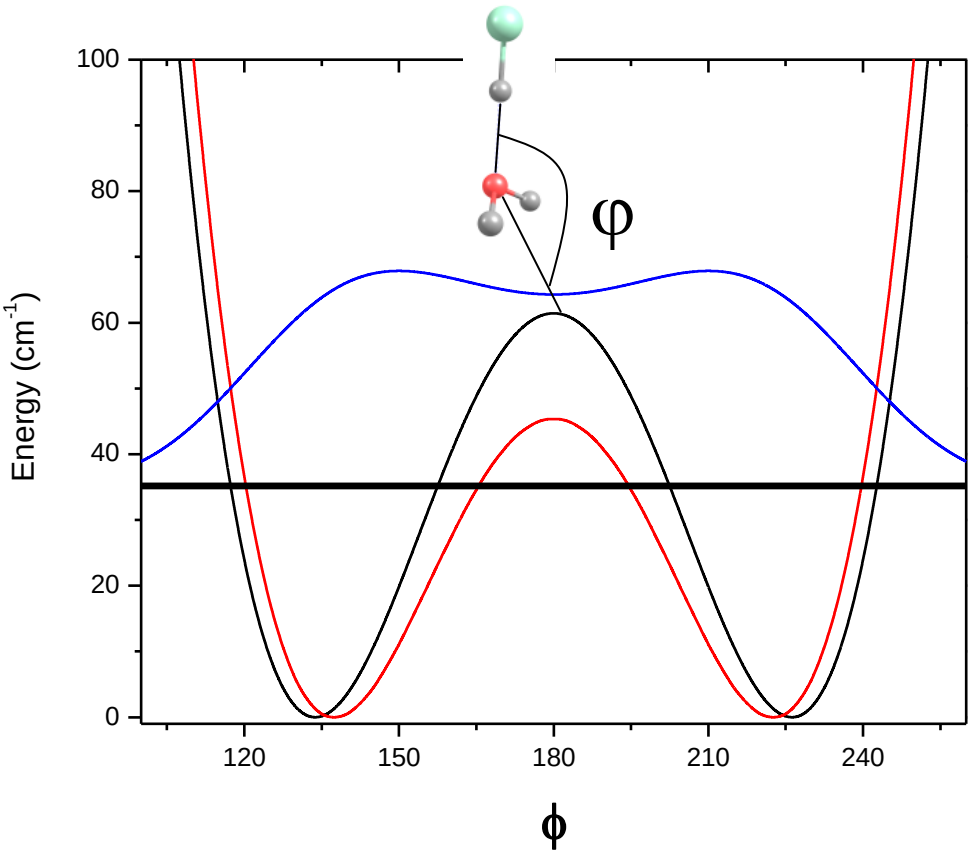

Figure 4.4 Calculated Change of Energy Based on Bond Angle Change. The black curve corresponds to the out of plane bending potential obtained at the MP2 / 6-311+g(3df,3pd) level of theory. A counterpoise correction was applied and all other degrees of freedom were relaxed at each value of φ. The Numerov method was used to obtain the zero-point level (37 cm^{-1}) and the wavefunction (blue curve). The dipole moment components and the VTMA of the HCl stretch was computed at each value of φ. The expectation values of μ_b and μ_c are assumed to be zero, due to symmetry. The expectation values of μ_a and the VTMA are determined in the usual way. Here the a, b, c labels denote the inertial axis. By including the dipole-induced helium polarization term in the potential, the barrier is reduced by 9.2 cm^{-1} (red curve). The zero-point level in this modified potential is at 32 cm^{-1}. Overall, the effect of the helium is to confine the complex to a more planar geometry.

In the previous FTIR free jet study,[21j] the S1 band at 2757 cm^{-1} was assigned to the 2:1 cluster shown in Figure 1.1. A second band labeled S8 was observed at 2580 cm^{-1} and was also assigned to this complex. The higher frequency S1 band was attributed to the Cl-H···Cl stretch, and the lower frequency S8 band was assigned to the Cl-H···O stretch. These assignments are in good agreement with the frequency shift predictions from the CCSD(T) calculations of the same authors.[21j] We did not find a band in the helium droplet spectrum near 2757 cm^{-1} that can be assigned to the 2:1 cluster; instead, at this frequency, there is a weak feature present that grows in intensity with increasing HCl PUC pressure and appears to be associated with a 3:1 cluster. However, we observe an intense band at 2774 cm^{-1} that does have a PUC pressure dependence that is consistent with the 2:1 assignment. We have labeled this band S0. It should be noted here that spectral features from pure $(HCl)_m$ clusters are also present in this range, with the $(HCl)_4$ cluster being observed previously at 2776 cm^{-1} in the gas phase[21j] and at 2773 cm^{-1} in helium droplets.[53]

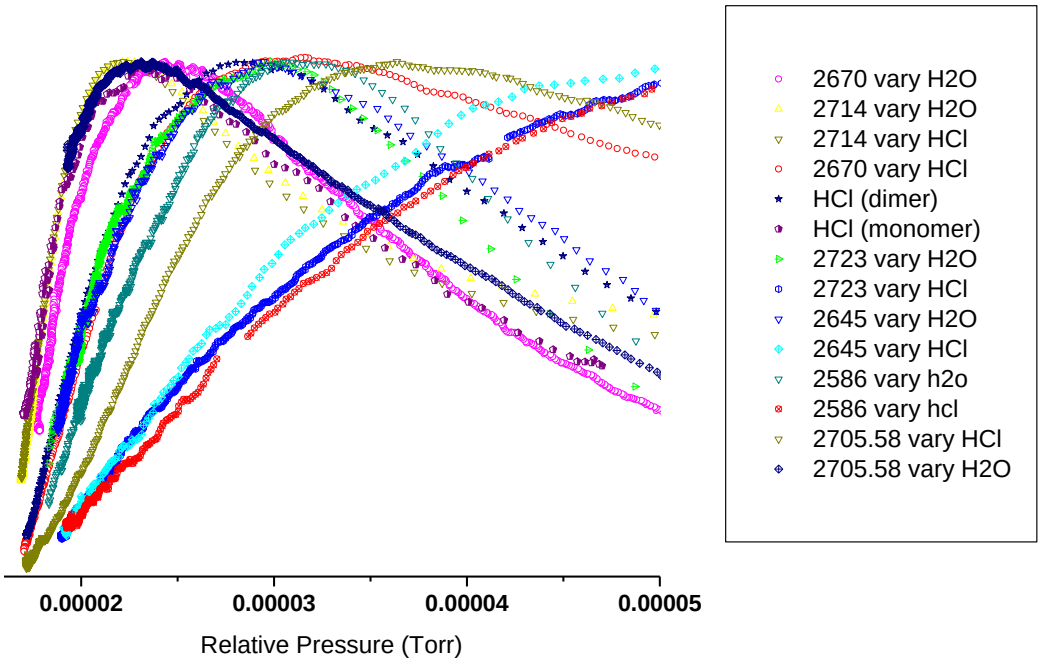

Figure 4.5 PUC Dependence of Different HCl-Water Clusters. The pick-up cell (PUC) pressure dependence with the laser frequency fixed to the peak of each of the sharp resonances and also on two different frequencies corresponding to the broad background (2645 and 2586 cm^{-1}) are shown. Each of the curves is initially offset by some background pressure, which can be different for each curve. So, what we do is to simply consider the *leading edges* of the PUC curves. Each curve is normalized so that the peak is at one. Also, the curves are translated so that the low pressure data all extrapolate to the same initial pressure value ($p_{initial}$). As seen in the figure above, all of the curves extrapolate to the same pressure, and the curves naturally fall into groups that have similar *leading edge slopes*. It is these *leading edge slopes* that we use to arrive at initial assignments of the spectra to a particular cluster size. We start by considering the slopes of the HCl monomer and HCl dimer curves. Comparing to these, we see that the band at 2714 cm^{-1} has a H_2O *and* HCl pressure dependence that have the same leading edge slopes as the HCl monomer curve. This, of course, was expected given the previous assignment of this band to the HCl-(H_2O) binary complex. Using the same logic, we arrive at the following assignments for cluster composition:

Wavenumber (cm^{-1})	**Compostion of the cluster responsible**
2774	2 HCl and 1 H_2O
2723	>3 HCl and 2 H_2O
2714	1 HCl and 1 H_2O
2705	3 HCl and 1 H_2O
2670	2 HCl and 2 H_2O
2645	3 HCl and >2 H_2O
2586	3 HCl and >2 H_2O

Table 4.1 Tabulated Results of PUC Study. The PUC dependency studies are summarized here to help identify what molecular clusters are responsible for the band probed, shown to the left in wavenumbers.

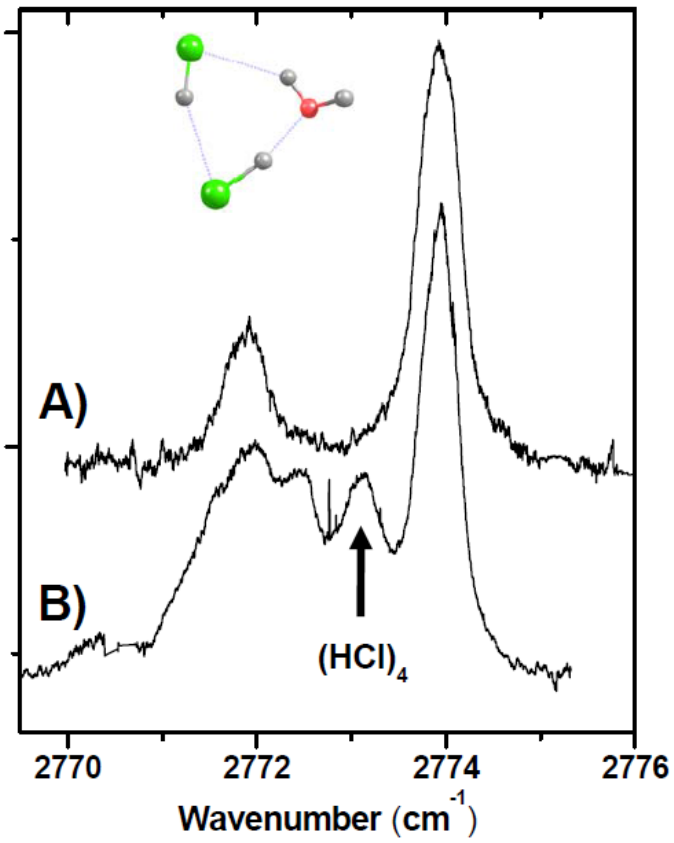

Figure 4.6 Comparison of Spectra Scanned on Different Mass Channels at 2774 cm ¯1. Two blown up spectra of the S0 band. A) scanned on m/z=19amu B) scanned RF only so all masses greater than 6amu are recognized for the purpose of ion selection. Scanning on mass 19 amu channel is primarily looking at hydronium ions, and so the signal from the HCl multimers is eliminated.

Figure 4.6 shows an expanded view of the S0 band region. Here the PUC pressures were kept somewhat lower to minimize signal contributions from the broad background. For the bottom spectrum (Fig 4.4B), the mass spectrometer was set to detect all masses greater than 6 u. As a result of this, the spectrum is a summation of all cluster absorption bands that fall in this region, including the pure $(HCl)_4$ band at 2773.1 cm^{-1} and a broader feature centered near 2772 cm^{-1} that is likely associated with other pure $(HCl)_m$ clusters. The top spectrum (Fig 4.6A) was recorded with the mass spectrometer fixed to 19 u. Since this mass corresponds to the H_3O^+ fragment ion signal, the excitation

of pure $(HCl)_m$ clusters cannot contribute to a signal modulation in this mass channel. Therefore, the top spectrum can only consist of bands from mixed $(HCl)_m(H_2O)_n$ clusters. More specifically, the two bands are assigned to an isotope splitting of the Cl-H···Cl stretch of the 2:1 cluster.

An analysis of this isotope splitting is shown in Figure 4.7. The inset shows the structure of the 2:1 cluster with each Cl atom labeled as **1** or **2**. The top black trace is the experimental spectrum recorded in mass channel 19 u. Two bands are observed at 2771.87 and 2773.91 cm^{-1}, which have an approximately 1:3 intensity ratio. Consistent with the observed splitting, *ab initio* calculations predict a 2.2 cm^{-1} redshift of the Cl-H···Cl stretch when the Cl atom labeled **1** is changed from ^{35}Cl to ^{37}Cl. In comparison, if the Cl atom labeled **2** is changed from ^{35}Cl to ^{37}Cl, a 0.02 cm^{-1} redshift is predicted. Also shown are four Lorentzian functions centered according to the predicted isotope shifts. Each Lorentzian has a 0.57 cm^{-1} linewidth and an area that is based on the 3:1 natural abundance of the ^{35}Cl: ^{37}Cl isotopes. The green trace has an area of 9 and corresponds to the isotopomer with two ^{35}Cl atoms. Each peak in the blue trace has an area of 3, with the higher frequency peak corresponding to **1**=^{35}Cl / **2**=^{37}Cl and the lower frequency peak corresponding to **1**=^{37}Cl / **2**=^{35}Cl. The lower navy trace has an area of 1 and corresponds to the isotopomer with two ^{37}Cl atoms. Consistent with the isotope assignment, the red smooth curve, which is the sum of the four Lorentzians, has a 1:3 intensity ratio and is in excellent agreement with experiment.

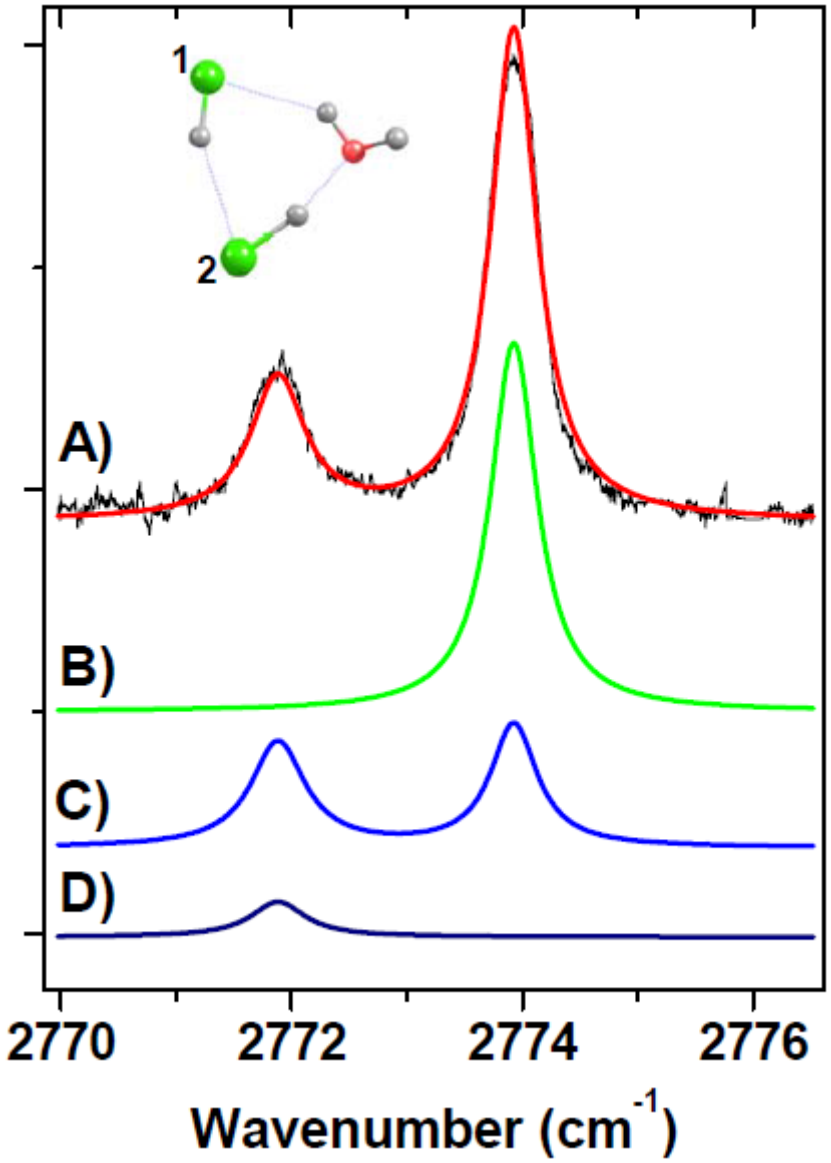

Figure 4.7 Isotopic Abundance of Cl Agrees with Experimental Spectrum. Experimental and theoretical spectra showing evidence that the two observed peaks are the same band, but from two different isotopomers. Using the natural isotopic abundance of Cl, a Lorentzian curve is predicted as a peak for each of the isotopomers. D) shows the predicted spectrum of the complex with two ^{37}Cl isotopes. C) is the predicted peaks for mixed isotopomers where each of the two possibilities are of mixed isotopomers. B) represents the case where both Cl atoms are mass 35 amu. The black line in part A) is an experimentally obtained spectrum. The red line is the sum of lines D, C, and B, and the agreement is very nice.

The PUC pressure dependence and the isotope splitting provide rather firm support for the assignment of the S0 band to the Cl-H···Cl stretch of the 2:1 cyclic

complex (Fig 1.1B). A more definitive assignment comes from the field dependence of the band intensity. As shown in Figure 4.8, applying the Stark field results in a signal change that is qualitatively different from that observed for the HCl stretch of the 1:1 complex. Specifically, the parallel polarization alignment leads to a *decrease* in intensity, whereas an increase is observed with the perpendicular alignment. Moreover,

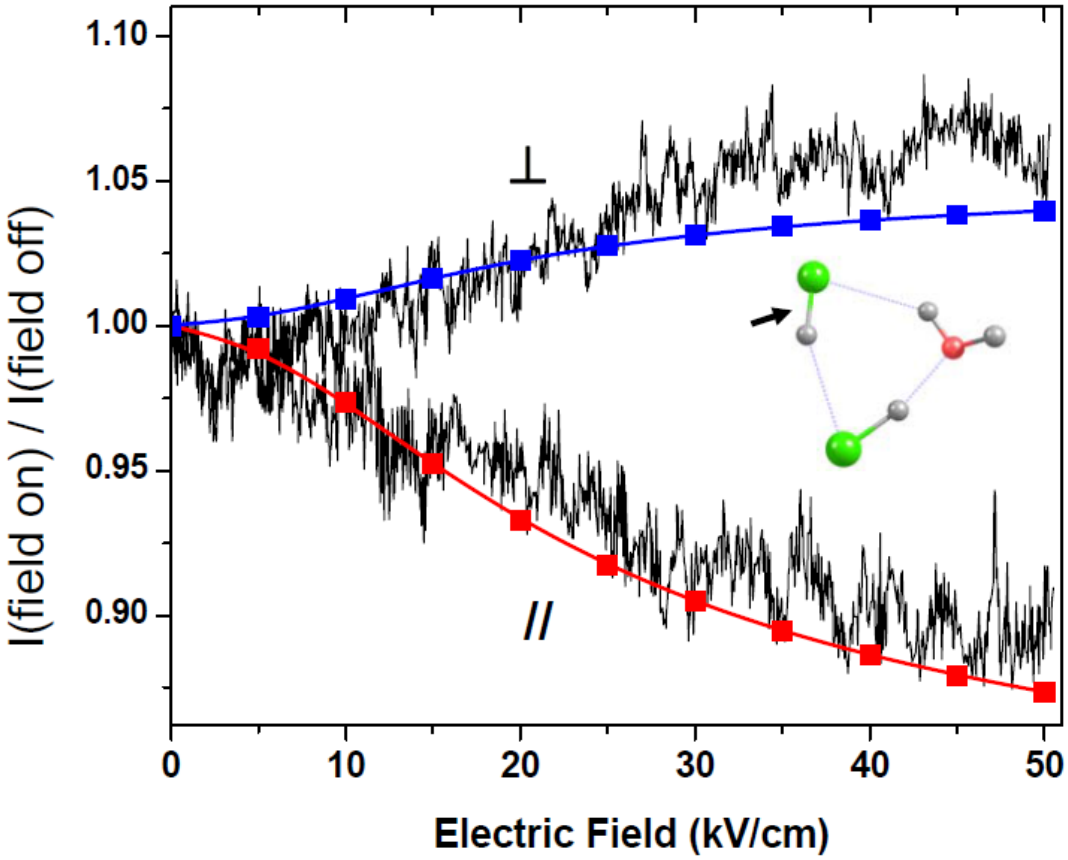

Figure 4.8 VTMA at 2774 cm^{-1}. Plot of signal change as a function of the electric field strength as the Stark field is applied at varying voltages, the laser is maintained at 2774 cm^{-1}, and the detection scheme is set to rf only. The blue and red lines represent the predicted perpendicular and parallel behavior of the signal relative to the applied field. The predictions are based on the molecular structure shown above with a VTMA of 62.3° and a dipole moment of 2.39 D using MP2 theory.

the signal change is less than 10 percent of the zero-field value. Both of these observations are consistent with a VTMA that is slightly larger than the magic angle

(54.75º), namely the VTMA corresponding to no field dependence.[17c] For comparison, the *ab initio* VTMA for the Cl-H···Cl stretch of the 2:1 cluster is 62.3º and μ_{MP2}=2.39 D. The field ON:OFF intensity ratio is simulated using the constants (μ_p=2.4 D, α=59.5º), and the overall agreement provides considerable support to the above assignment. Therefore, it is now safe to update the previous gas phase assignment of the 2:1 cluster from the S1 band to the S0 band. The Cl-H···O stretch is predicted to be redshifted 266 cm^{-1} from the Cl-H···Cl stretch; according to the gas phase study,[21j] this transition was observed as a 20 cm^{-1} broad band centered at 2580 cm^{-1}. Unfortunately, our wavelength range prohibits a further study of this band.

$\underline{(HCl)_2(H_2O)_2}$

In the gas phase study of Fárník et. al.,[21j] the S2, S4, and S5 bands were not assigned, but they did speculate as to the assignment of S5, based on the HCl/H_2O concentration dependence of their spectra. They stated, "While we cannot offer a plausible cluster assignment for S5, it appears to originate from a less HCl rich cluster, such as $(HCl)_2(H_2O)_2$, but clearly not from its alternating cyclic isomer." Our PUC results are consistent with this suggestion, and indeed, since the alternating cyclic isomer has predicted HCl stretch bands well below 2670 cm^{-1},[21f] an initial assignment of the S5 band to the non-alternating cyclic $(HCl)_2(H_2O)_2$ structure is certainly reasonable.

In a recent helium droplet study of $(HCl)_m(H_2O)_n$ clusters, an alternative assignment of the S5 band was presented.[28] Based on PUC measurements and OSMS, the 2670 cm^{-1}, S5 band was assigned to the symmetric hydronium stretch in the protolytically dissociated $H_3O^+(H_2O)_3Cl^-$ cluster.[28] This is an intriguing assignment given that four water molecules is the predicted minimum number necessary for the

dissociation of HCl in its ground vibrational state. [21b, 21c, 21e, 21f, 21h, 22a] It is important to emphasize here, however, that our PUC data is inconsistent with the assignment of the S5 band to the $H_3O^+(H_2O)_3Cl^-$ ion pair. As we increase the water pressure to a level that favors the formation of the 1:4 cluster, we only observe an increase in the broad feature that lies underneath the sharper S5 band. Once again, our data supports an initial assignment of the sharp S5 band to a 2:2 cluster. Possible candidate structures for this 2:2 cluster are given in Figures 1.1**C**-1**F**, and the *ab initio* frequency shifts, dipole moments, and VTMAs of these structures are summarized in Table 4.2.

TABLE 1: Experimental Constants Compared to Those from MP2/6-311+g(3df,3pd) Calculations[a]

experiment	$\Delta\nu$ (cm^{-1})	μ_p (D)	α (°)	PUC
S0	111	2.4(1)	59.5(8)	2:1
S1	126			3:1
S3	171	3.9(1)	0.0	1:1
S4	180		>80	3:1
S5	215	2.76(5)	58.2(2)	2:2
Ab Initio	$\Delta\nu$ (cm^{-1})	μ_p (D)	α (°)	*m:n*
A (C_s)	246	3.67	19.2	1:1
B	148	2.39	62.3	2:1
C	587	2.37	90.0	2:2
D	595	0.0	n/a	2:2
E	273	2.76	58.4	2:2
F	139	2.82	72.5	2:2
$H_3O^+(H_2O)_3Cl^-$	137	4.22	36.6	1:4

Table 4.2 Comparison of Experimental and Theoretical Constants. Comparison of experimental measurements to *ab initio* calculations. S0-S5 represent the bands shown in Figure 4.1. The letters corresponding to theory relate to the structures shown in Figure 1.1. Δυ refers to the frequency shift from the monomer in He droplets. The theoretically predicted values come from calculations at the MP2/6-311+g(3df,3pd) level.

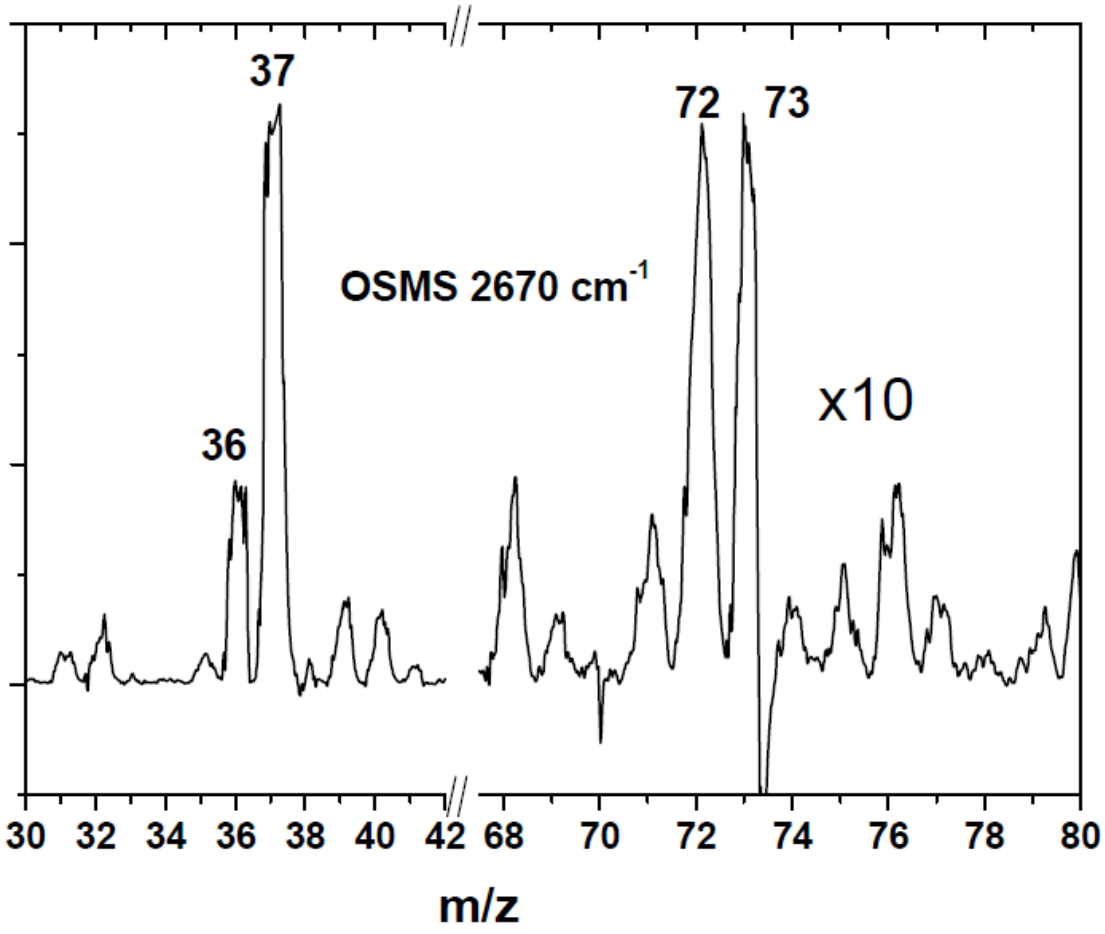

Figure 4.9 OSMS at 2670 cm^{-1}. The OSMS spectrum obtained with the radiation fixed at 2670.0 cm^{-1}. Most notably are the peaks at 36 and 37 m/z and refer to the $(H^{35}Cl)^+$, $H^+(H^{35}Cl)$ or $H^+(H_2O)_2$ ions respectfully. $(H^{35}Cl)_2^+$, and $H^+(H^{35}Cl)_2$ ions show up as masses 72 and 73, shown with an intensity ten times that of the first section of the OSMS.

Figure 4.9 shows the OSMS spectrum obtained with the OPO at 2670.0 cm^{-1}, corresponding to the peak of the S5 band. The mass spectrometer signal is processed with a lock-in amplifier, leading to a mass spectrum of only those species in resonance with the OPO frequency. For this measurement, we reduced the PUC pressures well below the levels required to optimize the intensity of the S5 band. Hence, the OSMS shown in Figure 4.9 is only representative of the cluster associated with the S5 band and not the clusters (either dissociated or undissociated) that contribute to the underlying

broad background in this spectral region. The most intense peaks in the OSMS are 19, 36, 37, 72, and 73 u. We assign these to H_3O^+, $(H^{35}Cl)^+$, $H^+(H^{35}Cl)$ or $H^+(H_2O)_2$, $(H^{35}Cl)_2^+$, and $H^+(H^{35}Cl)_2$, respectively. These assignments are motivated by and are consistent with the suggested S5 band assignment of Fárník et. al.,[21j] i.e. the non-alternating cyclic $(HCl)_2(H_2O)_2$ cluster (Fig. 1**E**). On the other hand, the OSMS is not consistent with the assignment of S5 to the $H_3O^+(H_2O)_3Cl^-$ species. Indeed, the strong signals at both 36 and 72 u indicate intact HCl molecules following ionization and fragmentation of the cluster, and it is not clear how these can arise from the $H_3O^+(H_2O)_3Cl^-$ solvent separated ion pair.

Figure 4.10 shows an expanded view of the S5 band. The spectrum in Figure 4.10A is obtained with the mass spectrometer tuned to 19 u, which corresponds to H_3O^+. In the 19 u spectrum, the S5 band is split into two peaks centered at 2667.9 and 2670.0 cm^{-1}. In the previous report,[28] the weaker band at 2667.9 cm^{-1} was assigned to a nearly isoenergetic isomer of the $H_3O^+(H_2O)_3Cl^-$ species. By tuning the mass spectrometer to 72 u $(H^{35}Cl)_2^+$ (Figure 4.8B), the band at 2667.9 cm^{-1} disappears, while the 2670.0 cm^{-1} band remains. This observation is consistent with an assignment of the two observed bands to the expected isotope splitting in the spectrum of $(HCl)_2(H_2O)_2$ (Fig. 1.1**E**) due to the ^{35}Cl: ^{37}Cl 3:1 isotope ratio, analogous to the splitting observed for the S0 band associated with the 2:1 cluster. Once again, *ab initio* calculations predict a 2 cm^{-1} redshift of the Cl-H···Cl stretch when the Cl atom labeled with a **1** is changed from ^{35}Cl to ^{37}Cl (Fig. 4.10 inset), consistent with the experimentally observed splitting. Figure 4.11 shows an

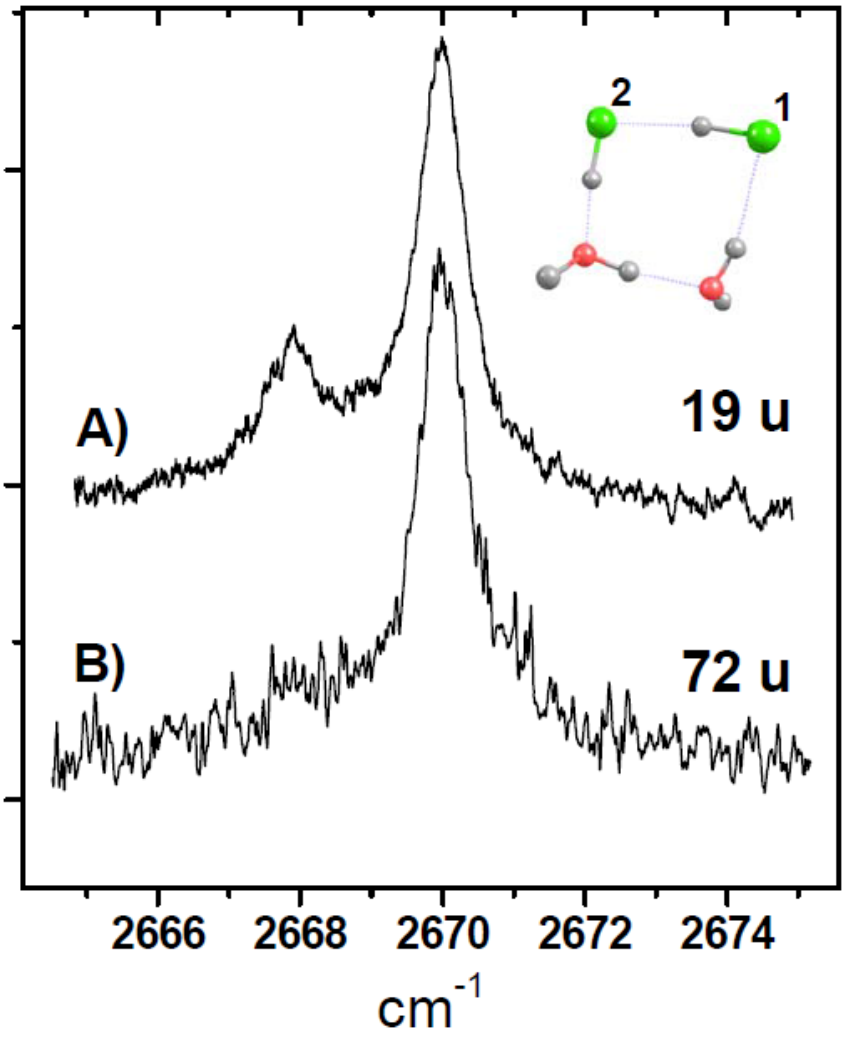

Figure 4.10 High Resolution Spectra of $(HCl)_2(H_2O)_2$. Two spectra A) and B), which are scans of the same region, but on different mass channels as indicated in the figure above. By scanning on mass 19 amu, the hydronium ion, signal from both isotopomers are present. By scanning on mass 72 the signal from $H^{37}Cl$ structures is nearly eliminated.

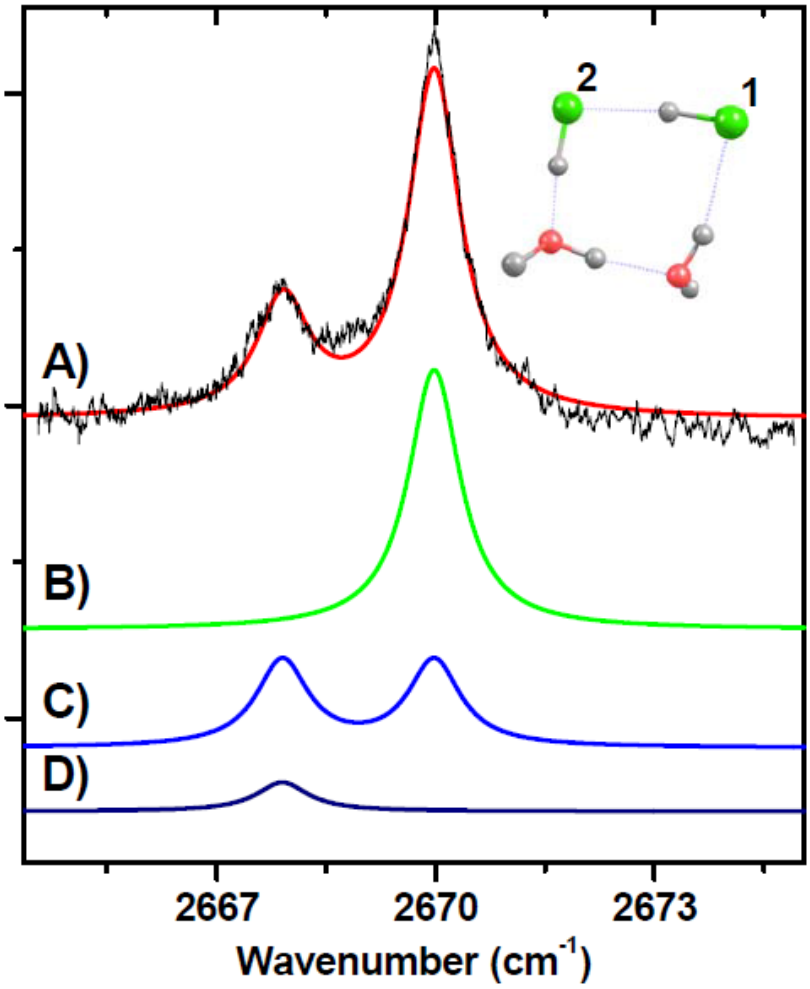

Figure 4.11 Evidence for Isotopic Splitting Based on NIA of Cl. The isotopic splitting of the S5 band from Figure 4.1 is confirmed by comparing experimental results to theoretical predictions. The methodology used here is identical to that in Figure 4.7.

analysis of this isotope splitting, where similar to the above discussion for the 2:1 cluster, the green, blue, and navy curves correspond to **1**,**2**=^{35}Cl, **1**=^{35,37}Cl / **2**=^{37,35}Cl, and **1**,**2**=^{37}Cl, respectively. The smooth red trace is the summation of the three curves, which is in excellent agreement with the observed splitting and intensity ratios. Certainly, in combination, the PUC cell dependence, the OSMS, and the isotope analysis all provide considerable support to the assignment of S5 to the 2:2 cluster shown as structure **E** in

Figure 1.1. Nevertheless, given the disagreement with the previous study,[28] we felt that it was imperative to have additional evidence for our assignment.

For a definitive assignment of the S5 band, we turn to the electric field dependence. The electric field dependence of the intensity is shown in the top panel of Figure 4.12. Here the mass spectrometer detection channel is 19 u, and the OPO frequency is set to 2670.0 cm^{-1}. With the parallel polarization alignment, the signal intensity decreases as the Stark field increases. In comparison, a small increase in signal intensity is observed when the laser electric field is aligned perpendicular to the Stark field.[58] Qualitatively, both of these results indicate that the VTMA for the vibration probed here is greater than 54.75°.[17c] The simulated field dependences are shown as squares in Figure 11; here the blue and red points correspond to perpendicular and parallel polarizations, respectively. The value of the VTMA (α=58.2 °) was adjusted to give the best agreement with the experiment. As shown in Figure 1.1, for structure **E**, the *ab initio* VTMA for the Cl-H···Cl stretch is 58.4 °, which is in excellent agreement with the experiment. Furthermore, the predicted field dependences for the other calculated 2:2 structures are in qualitative disagreement with the experimental measurements. Simulations of the field dependence for structures **C** through **F** are shown in the bottom panel of Figure 11. Note that there is no field dependence for structure **D**, given that it is non-polar. For completeness, we have also simulated the field dependence for the protolytically dissociated $H_3O^+(H_2O)_3Cl^-$ cluster. This species has a much larger dipole moment (4.22 D) than that required to satisfactorily simulate the experimental field dependence. Furthermore, if we assume the VTMA calculated for the symmetric hydronium stretch of $H_3O^+(H_2O)_3Cl^-$ (36.6°), a qualitatively wrong trend is predicted for

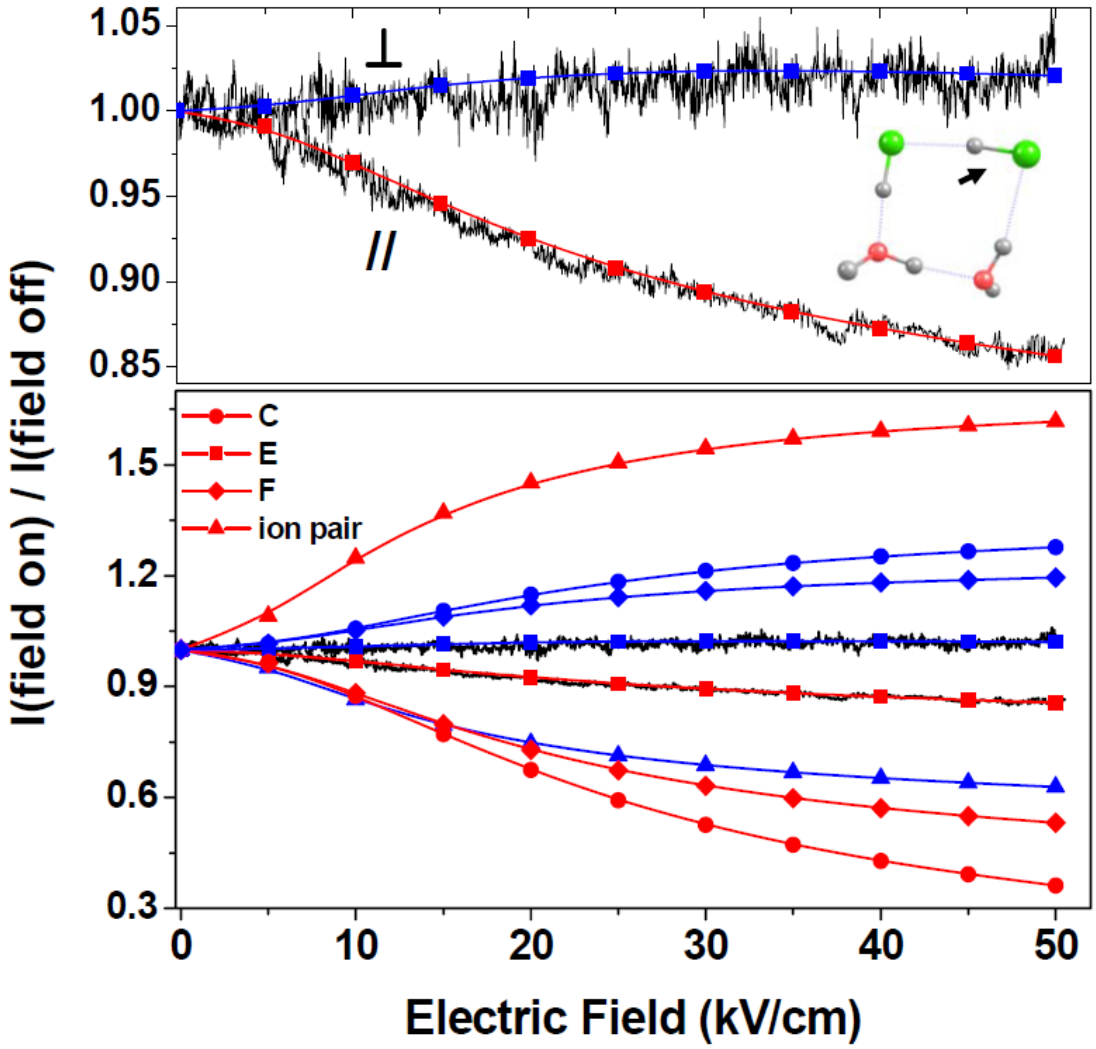

Figure 4.12 VTMA of multiple HCl-Water Structures. Top Panel: Electric field On vs Off dependence of the signal intensity at 2670.0 cm^{-1}. The detection channel is 19 amu. The black traces are experimentally obtained at perpendicular and parallel light polarizations as shown above. The red trace shows the predicted parallel trend, while the blue line shows the corresponding perpenduclarly polarized case. The band excited is denoted by an arrow. C, E, and F refer to the structures in Figure 1.1. The ion pair suggested by Havenith is shown as triangles. Structure E agrees with experiment the best as marked by squares. The structure that is least likely was for the previously claimed ion pair.

the signal intensity as the field increases. That is, with parallel polarization, an increase in signal is predicted, rather than the observed decrease. Clearly, the agreement between

theory and experiment for structure **E** provides rather definitive support to our assignment of the S5 band to the non-alternating, cyclic $(HCl)_2(H_2O)_2$ cluster. For the Cl-H···O stretch transition of this cluster, a 526 cm^{-1} redshift is predicted from the S5 band, placing it well outside of the tuning range of our OPO.

Larger Clusters

Two other pronounced bands in the survey spectrum shown in Figure 4.1 are those at 2705 and 2721 cm^{-1}. The PUC pressure dependence of these bands leads us to tentatively assign these to a Cl-H···Cl type stretch in a 3:1 and a 4:2 cluster, respectively. Unfortunately, at the higher PUC pressures required to optimize these bands, the broad background becomes more pronounced, making a definitive assignment based on the field dependence more difficult. Moreover, these bands are partially overlapped with the HCl stretch band of the 1:1 complex. Nevertheless, as shown in Figure 4.13, the field dependence of the 2705 cm^{-1} band is in qualitative agreement with simulations based on the VTMA (73.9 º) of the lower frequency Cl-H···Cl stretch vibration of the cyclic $(HCl)_3(H_2O)$ cluster. The higher frequency Cl-H···Cl stretch of this cluster may be the feature at 2757 cm^{-1} discussed above (S1) that was previously assigned to the 2:1 cluster in the FTIR free jet spectrum.[21j] Once again, the Cl-H···O stretch of this species is predicted to be redshifted outside our tuning range.

Between 2750 and 2825 cm^{-1}, there are several weak but reproducible features that are associated with larger clusters. We speculate here that these are due to Cl-H···Cl stretches in larger mixed $(HCl)_m(H_2O)_n$ clusters, including branched clusters that have dangling HCl moieties. Indeed, in the spectra of helium solvated pure $(HCl)_n$ clusters,

this region of the spectrum became congested and grew in intensity with increasing HCl pressure.[53] Although the global minima are cyclic, low-lying branched structures are

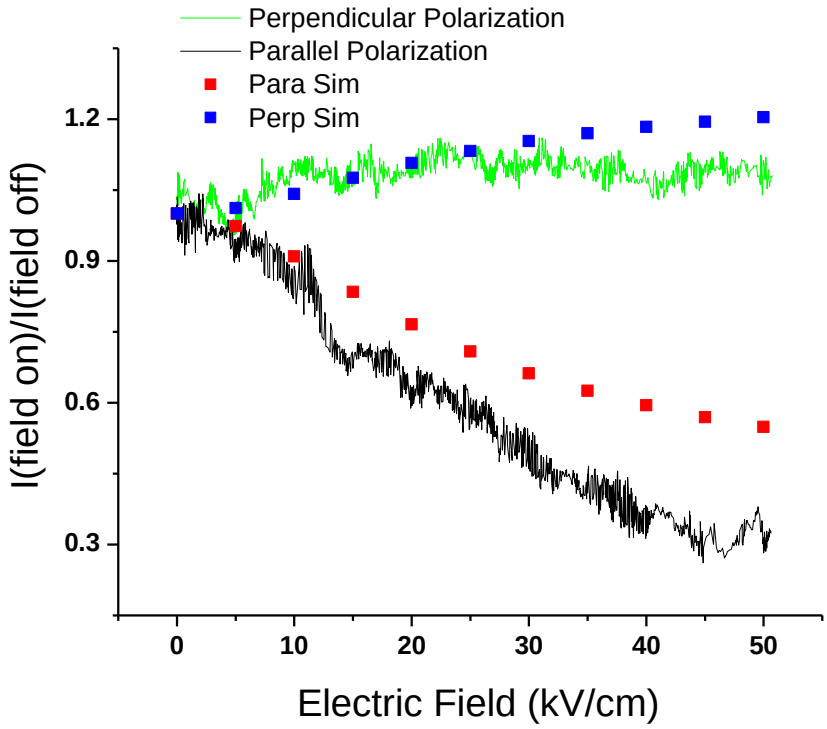

Figure 4.13 VTMA of Band at 2705 cm^{-1}. Electric field dependence plot of the 2705 cm^{-1} band. The black trace is the experiment with parallel polarization; the green trace is the experimentally obtained data with perpendicular polarization. The predicted field dependence is shown for the structure of the 3:1 species, in Figure 1.1, as squares and agrees marginally well with the experimental data. It doesn't agree as well as previous examples. This deviation is due to larger clusters that have broad signal that grows in as background signal increases in the same region.

predicted as energetic minima for $(HCl)_n$ clusters with n>4, and these have Cl-H···Cl stretches that are spread throughout the 2700-2850 cm^{-1} range.[53] Similar chromophores in mixed $(HCl)_m(H_2O)_n$ clusters could potentially contribute to a broad background in this

region, given the diversity of cluster structures with increasing cluster size and the tendency of locally stable structures to be stabilized in the helium environment.[17b, 59] Indeed, a broad background in the HCl stretch region is observed in both the gas phase [21j, 26] and helium droplet spectra [29, 60] of $(HCl)_m(H_2O)_n$. Moreover, broad bands in this region have been observed in the spectra of HCl on the surface of nanometer ice particles.[19a, 19b, 20d] The origin and significance of this broad background, common to all three measurements, has been described in more detail in a previous report.[29] We note again that the PUC dependence of the signal at 2580 and 2640 cm^{-1} indicates that the broad background observed in this study arises from $(HCl)_m(H_2O)_n$ clusters with m>3 and n>2.

Conclusions

The helium nanodroplet isolation spectra of $(HCl)_m(H_2O)_n$ clusters have been measured in the Cl-H···Cl range. The combination of pick-up cell pressure dependence, optically selected mass spectrometry, and electric field dependence measurements have lead to definitive assignments of the sharp bands observed in this region. Bands associated with the 1:1 binary complex and the 2:1, 2:2, and 3:1 clusters are observed at 2715, 2774, 2670, and 2705 cm^{-1}, respectively. Each of these bands are split due to the presence of a distribution of isotopomers. These splittings are accurately reproduced assuming the 3:1 natural abundance of ^{35}Cl: ^{37}Cl isotopes. Simulations of the electric field dependence of these bands allow us to make definite structural assignments despite the lack of rotational fine structure in the spectra of these species. The field dependence of the HCl stretch band associated with the 1:1 cluster indicates a vibrationally averaged C_{2v} structure, in agreement with previous studies. We have confirmed that the 2:1 cluster

is cyclic and that the 2:2 cluster has a non-alternating cyclic structure. The broad background observed in previous measurements of these clusters in various environments has been similarly observed here. The pressure dependence of this broad background suggests that it originates at least partially from mixed $(HCl)_m(H_2O)_n$ clusters with m>3 and n>2.

References

1. Onnes, H. K., *Commun. Phys. Lab. Univ. Leiden* **1908,** *108* (3).

2. Becker, E. W.; Klingelhofer, R.; Lohse, P., *Z Naturforsch Pt A* **1961,** *16* (11), 1259-1259.

3. Harms, J.; Toennies, J. P.; Knuth, E. L., *J. Chem. Phys.* **1997,** *106* (8), 3348-3357.

4. Choi, M. Y.; Douberly, G. E.; Falconer, T. M.; Lewis, W. K.; Lindsay, C. M.; Merritt, J. M.; Stiles, P. L.; Miller, R. E., *Int. Rev. Phys. Chem.* **2006,** *25* (1-2), 15-75.

5. Toennies, J. P.; Vilesov, A. F., *Angew. Chem. Int. Ed.* **2004,** *43* (20), 2622-2648.

6. Whittle, E., D. A. D., Pimentel, G. C., *J. Chem. Phys* **1954,** *22,* 1943-1946.

7. T. E. Gough, M. M., P. A. Rowntree, and G. Scoles, *J. Chem. Phys.* **1985,** *83*, 4958-4962.

8. Goyal, S.; Schutt, D. L.; Scoles, G., *Phys. Rev. Lett.* **1994,** *73* (18), 2512-2512.

9. Gough, T. E., D. G. K., and Scoles, G., *Chem. Phys. Lett.* **1983,** *97,* 155-160.

10. Goyal, S., G. N. R., D. L. Schutt, and Scoles, G., *J. Phys. Chem.* **1991,** *95,* 4186.

11. Ehbrecht, M., and Huisken, F., *J. Phys. Chem. A* **1997,** *101,* 7768-7777.

12. Brink, D. M.; Stringari, S., *Z. Phys. D* **1990,** *15* (3), 257-263.

13. Frochtenicht, R.; Toennies, J. P.; Vilesov, A., *Chem. Phys. Lett.* **1994,** *229,* 1-7.

14. Stienkemeier, F.; Lehmann, K. K., *J. Phys. B* **2006,** *39* (8), R127-R166.

15. Callegari, C.; Lehmann, K. K.; Schmied, R.; Scoles, G., *J. Chem. Phys.* **2001,** *115* (22), 10090-10110.

16. (a) Bondybey, V. E.; Beyer, M. K., *Int. Rev. Phys. Chem.* **2002,** *21* (2), 277-306.

17. (a) Zonnevylle, M. C.; Geerlings, J. J. C.; Vansanten, R. A., *J. Catal.* **1994,** *148* (2), 417-426; (b) Toennies, J. P.; Vilesov, A. F., *Annu. Rev. Phys. Chem.* **1998,** *49,* 1-41; (c) Hermann, K.; Bagus, P. S.; Bauschlicher Jr., C. W., *Phys. Rev. B* **1984,** *30* (12), 7313-7316.

18. Slipchenko, M. N.; Vilesov, A. F., *Chem. Phys. Lett.* **2005,** *412* (1-3), 176-183.

19. (a) Buch, V.; Sadlej, J.; Aytemiz-Uras, N.; Devlin, J. P., *J. Phys. Chem. A* **2002,** *106* (41), 9374-9389; (b) Vissers, G. W. M.; McCoy, A. B., *J. Phys. Chem. A* **2006,** *110* (18), 5978-5981.

20. (a) Douberly, G. E.; Merritt, J. M.; Miller, R. E., *Phys. Chem. Chem. Phys.* **2005,** *7* (3), 463-468; (b) Kwon, Y.; Whaley, K. B., *J. Phys. Chem. Solids* **2005,** *66,* (8-9), 1516-1519; (c) Kwon, Y.; Whaley, K. B., *J. Low Temp. Phys.* **2005,** *140* (3-4), 227-240; (d) Walker, K. A.; Evans, C. J.; Suh, S. H. K.; Gerry, M. C. L.; Watson, J. K. G., *J. Mol. Spectrosc.* **2001,** *209* (2), 178-191.

21. (a) Packer, M. J.; Clary, D. C., *J. Phys. Chem.* **1995,** *99* (39), 14323-14333; (b) Paesani, F.; Gianturco, F. A.; Whaley, K. B., *J. Chem. Phys.* **2001,** *115* (22), 10225-10238; (c) Re, S.; Osamura, Y.; Suzuki, Y.; Schaefer, H. F.,*J. Chem. Phys.* **1998,** *109* (3), 973-977; (d) Huang, W.; Zhai, H. J.; Wang, L. S., *J. Am. Chem. Soc.* **2010,** *132* (12), 4344-4351; (e) Koszinowski, K.; Schroder, D.; Schwarz, H., *Organometallics* **2004,** *23* (5), 1132-1139; (f) Chaban, G. M.; Gerber, R. B.; Janda, K. C., *J. Phys. Chem. A* **2001,**

105 (36), 8323-8332; (g) Neukermans, S.; Veldeman, N.; Janssens, E.; Lievens, P.; Chen, Z.; Schleyer, P. V. R., *Eur. Phys. J. D* **2007,** *45* (2), 301-308; (h) Cabaleiro-Lago, E. M.; Hermida-Ramon, J. M.; Rodriguez-Otero, J., *J. Chem. Phys.* **2002,** *117* (7), 3160-3168; (i) Stiles, P. L.; Miller, R. E., *J. Phys. Chem. A* **2006,** *110* (17), 5620-5628; (j) Masia, M.; Forbert, H.; Marx, D., *J. Phys. Chem. A* **2007,** *111* (49), 12181-12191.

22. (a) Bacelo, D. E.; Binning, R. C.; Ishikawa, Y., *J. Phys. Chem. A* **1999,** *103* (24), 4631-4640; (b) Mitric, R.; Burgel, C.; Burda, J.; Bonacic-Koutecky, V.; Fantucci, P., *Eur. Phys. J. D* **2003,** *24* (1-3), 41-44.

23. (a) Lehmann, K. K., *J. Chem. Phys.* **2004,** *120* (2), 513-515; (b) Kisiel, Z.; Pietrewicz, B. A.; Desyatnyk, O.; Pszczolkowski, L.; Struniewicz, I.; Sadlej, J., *J. Chem. Phys.* **2003,** *119* (12), 5907-5917; (c) Lindinger, A.; Toennies, J. P.; Vilesov, A. F., *J. Chem. Phys.* **2004,** *121* (24), 12282-12292.

24. Glaspell, G.; Hassan, H. M. A.; Elzatahry, A.; Abdalsayed, V.; El-Shall, M. S., *Top. Catal.* **2008,** *47* (1-2), 22-31.

25. (a) Schmied, R.; Carcabal, P.; Dokter, A. M.; Lonij, V. P. A.; Lehmann, K. K.; Scoles, G., *J. Chem. Phys.* **2004,** *121* (6), 2701-2710; (b) Choi, M. Y.; Miller, R. E., *Phys. Chem. Chem. Phys.* **2005,** *7* (20), 3565-3573.

26. Reber, A. C.; Khanna, S. N.; Castleman, A. W., *J. Am. Chem. Soc.* **2007,** *129* (33), 10189-10194.

27. Yetter, R. A.; Risha, G. A.; Son, S. F., *P. Combust. Inst.* **2009,** *32*, 1819-1838.

28. Sullivan, K.; Young, G.; Zachariah, M. R., *Combust. Flame* **2009,** *156* (2), 302-309.

29. Paesani, F.; Zillich, R.; Kwon, Y.; Whaley, K. B., *Abstr. Pap. Am. Chem. S.* **2004,** *228,* U227-U227.

30. Gutberlet, A.; Schwaab, G.; Birer, O.; Masia, M.; Kaczmarek, A.; Forbert, H.; Havenith, M.; Marx, D., *Science* **2009,** *324* (5934), 1545-1548.

31. Nauta, K.; Miller, R. E., *Science* **2000,** *287* (5451), 293-295.

32. Kennedy, D.; Norman, C., *Science* **2005,** *309* (5731), 75-75.

33. Burnham, C. J.; Xantheas, S. S.; Miller, M. A.; Applegate, B. E.; Miller, R. E., *J. Chem. Phys.* **2002,** *117* (3), 1109-1122.

34. Kang, D.; Dai, J.; Hou, Y.; Yuan, J., *J. Chem. Phys.* **2010,** *133* (1), 014302-014309.

35. Xantheas, S. S., *Philos. Mag. B.* **1996,** *73,* 107-115.

36. (a) Nauta, K.; Miller, R. E., *J. Chem. Phys.* **2000,** *113* (22), 10158-10168; (b) Reho, J. H.; Merker, U.; Radcliff, M. R.; Lehmann, K. K.; Scoles, G., *J. Phys. Chem. A* **2000,** *104* (16), 3620-3626.

37. Reho, J.; Higgins, J.; Callegari, C.; Lehmann, K. K.; Scoles, G., *J. Chem. Phys.* **2000,** *113* (21), 9686-9693.

38. Lindinger, A.; Neumark, D. M.; Toennies, J. P.; Vilesov, A. F., *Abstr. Pap. Am. Chem. S.* **2000,** *220,* U209-U209.

39. Flynn, S. D.; Skvortsov, D.; Morrison, A. M.; Liang, T.; Choi, M. Y.; Douberly, G. E.; Vilesov, A. F., *J. Phys. Chem. Lett.* **2010,** 1, 2233-2238.

40. Morrison, A. M.; Flynn, S. D.; Liang, T.; Douberly, G. E., *J. Phys. Chem. A* **2010,** *114* (31), 8090-8098.

41. Morrison, A. M. Automation of an Aculight Optical Parametric Oscillator. University of Georgia, 2012.

42. Grebenev, S.; Lugovoi, E.; Sartakov, B. G.; Toennies, J. P.; Vilesov, A. F., *Faraday Discuss.* **2001,** *118*, 19-32.

43. Kwon, Y.; Whaley, K. B., *J. Chem. Phys.* **2001,** *115* (22), 10146-10153.

44. (a) Nauta, K.; Miller, R. E., *Chem. Phys. Lett.* **2001,** *350* (3-4), 225-232; (b) Lindinger, A.; Lugovoj, E.; Toennies, J. P.; Vilesov, A. F., *Z. Phys. Chem. Int. J. Res. Phys. Chem. Chem. Phy.* **2001,** *215*, 401-416.

45. Hartmann, M.; Toennies, J. P.; Vilesov, A. F.; Benedek, G., *Czech. J. Phys.* **1996,** *46*, 2951-2956.

46. Grebenev, S.; Sartakov, B.; Toennies, J. P.; Vilesov, A., *Phys. Rev. Lett.* **2002,** *89*, 225301-225305.

47. Toennies, J. P.; Vilesov, A. F.; Whaley, K. B., *Phys. Today* **2001,** *54* (2), 31-37.

48. Yoon, B.; Hakkinen, H.; Landman, U., *J. Phys. Chem. A* **2003,** *107* (20), 4066-4071.

49. Stolcic, D.; Fischer, M.; Gantefor, G.; Kim, Y. D.; Sun, Q.; Jena, P., *J. Am. Chem. Soc.* **2003,** *125* (10), 2848-2849.

50. Dong, F.; Miller, R. E., *Science* **2002,** *298* (5596), 1227-1230.

51. Choi, M. Y.; Dong, F.; Miller, R. E., *Philos. Trans. R. Soc. London Ser. a* **2005,** *363* (1827), 393-412.

52. Choi, M. Y.; Dong, F.; Han, S. W.; Miller, R. E., *J. Phys. Chem. A* **2008,** *112* (31), 7185-7190.

53. Nauta, K.; Miller, R. E., *J. Chem. Phys.* **2002,** *117* (10), 4846-4852.

54. van Heijnsbergen, D.; Jaeger, T. D.; von Helden, G.; Meijer, G.; Duncan, M. A., *Chem. Phys. Lett.* **2002,** *364* (3-4), 345-351.

55. (a) Behrens, M.; Buck, U.; Frochtenicht, R.; Hartmann, M.; Huisken, F.; Rohmund, F., *J. Chem. Phys.* **1998,** *109* (14), 5914-5920; (b) Bagus, P. S.; Hermann, K.; Bauschlicher Jr., C. W., *J. Chem. Phys.* **1984,** *80* (9), 4378-4386.

56. Kupper, J.; Merritt, J. M.; Miller, R. E., *J. Chem. Phys.* **2002,** *117* (2), 647-652.

57. Huisken, F.; Kaloudis, M.; Vigasin, A. A., *Chem. Phys. Lett.* **1997,** *269,* 235-243.

58. The electric field dependence is the same for both isotopomer bands (2667.9 and 2670.0 cm-1) within the experimental accuracy.

59. Close, J. D.; Federmann, F.; Hoffmann, K.; Quaas, N., *J. Low Temp. Phys.* **1998,** *111* (3-4), 661-676.

60. Portner, N.; Toennies, J. P.; Vilesov, A. F., *J. Chem. Phys.* **2002,** *117* (13), 6054-6060.

CHAPTER 5

Future Outlook

The future of HENDI is promising in the academic setting to help obtain basic spectra of molecules and molecular complexes at very low temperatures. HENDI allows for the formation of unique structures such as the "3+1" water structure that is observed for the first time here. There is quite a bit of work left to do to fully complete the Ne-H_2O study. Since the stabilization and isolation of higher energy structures is mostly due to sterics, it would be prudent to try other Noble gasses with larger radii to see if any other high energy small water clusters are formed. This can be easily accomplished by using gases such as Ar, Kr, or Xe instead of Ne and repeating the methods used here to investigate for new molecular structures.

The isolation of the H^+ Cl^- ion separated pair has proven very difficult for at least three different HENDI groups. The investigation of HCl-H_2O presented here was useful to confirm the previous assignments of others, to redefine an ill-assigned band, and to make an assignment to a previously unknown band. The outcome of the experiment suggests that the signal for the ion separated pair is likely present in the spectra, but it is mixed in with the broad background that grows with increasing water pressure. At this point, in the H-Cl stretch region, it is not possible to show the ion dissociated pair, nor at what number of water molecules is required to dissociate the HCl molecule. Unfortunately, the only way I predict the charge dissociated species will be positively identified is if a very precise droplet doping method is developed. Until then the

distribution of the number of water molecules in droplets causes a broad background that is comprised of many overlapping motions from different structures.

In addition to the Ne-H_2O and HCl-H_2O studies I have also spent quite a bit of time examining glycine. The groundwork for a water solvation study in He nanodroplets is laid out. There are now high resolution spectra and an abundance of mass spectral data on glycine in He nanodroplets. The ultimate goal would be to add water molecules to the glycine in order to form the zwitterion. It would be nice to know how many water molecules it takes to stabilize the zwitterion form of glycine that is always seen in aqueous solution. It should be noted, however, that the number of water molecules required to promote the zwitterion formation is likely very high. The large number of water molecules required to solvate the glycine zwitterion will make this difficult from an experimental view point. It would be better to find a different amino acid that could be vaporized without decomposing, and that has a better intramolecular stabilization energy, which would decrease the requisite number of waters for form the zwitterion.